THE ASTROPHYSICAL JOURNAL, 340:869–893, 1989 May 15

FAST MOLECULAR SHOCKS. I. REFORMATION OF MOLECULES BEHIND A DISSOCIATIVE SHOCK

DAVID A. NEUFELD AND A. DALGARNO
Harvard-Smithsonian Center for Astrophysics
Received 1988 May 5; accepted 1988 October 25

ABSTRACT

We discuss the physical and chemical processes that operate in the cooling gas behind a fast, dissociative, single-fluid shock propagating in a dense interstellar cloud. Our treatment extends previous theoretical work on fast molecular shocks by including the effects of the conversion of Lyα photons into radiation of the two-photon continuum and into H_2 Lyman band emission lines, the effects of CO photodissociation following line absorption, and the formation and destruction of molecules containing the elements nitrogen, silicon, and sulphur, and of the complex hydrocarbons. We present abundance profiles for the molecular species of interest. After molecular hydrogen begins to reform by means of gas phase and grain surface processes the neutral species OH, H_2O, O_2, CO, CN, HCN, N_2, NO, SO, and SiO reach substantial abundances. The molecular ions HeH^+, OH^+, SO^+, CH^+, H_2^+, and H_3^+, are produced while the gas is still hot and partially ionized. Emissions from them provide a possible diagnostic probe of fast molecular shocks.

Subject headings: interstellar: molecules — molecular processes — shock waves

I. INTRODUCTION

Observations of infrared emission from shock-heated molecular gas in the interstellar medium (e.g., Gautier *et al.* 1976; Bally and Lane 1982) have prompted serious attention to the theoretical problem of the structure of molecular shocks. Theoretical work (Draine 1980; McKee, Chernoff, and Hollenbach 1984) has shown that in the presence of magnetic fields of typical interstellar strength such shocks are of two types.

Shocks of velocity less than ~ 50 km s^{-1} are not fast enough to dissociate molecular coolants, with the result that the shocked gas cools on a time scale shorter than the ambipolar diffusion time and the ion and neutral fluids must be treated separately. Such "C"-type shocks—so-called because the physical parameters in both fluids change *continuously* (Draine 1980)—have received extensive theoretical study. Recent models of C-type shocks in *diffuse* interstellar clouds (Draine and Katz 1986; Draine 1986; Pineau des Forets *et al.* 1986, 1987; Pineau des Forets and Flower 1987) have included a large number of chemical processes involving many molecular species. C-type shocks in dense molecular clouds have been invoked very successfully (Chernoff, Hollenbach, and McKee 1982; Draine and Roberge 1982; Draine, Roberge, and Dalgarno 1983) to explain the H_2 $v = 1 \rightarrow 0$ (Beckwith *et al.* 1978) and high-J CO emission (Watson *et al.* 1985, and references therein) observed in Orion-KL, the best-studied shocked gas region.

Shocks of velocity greater than ~ 50 km s^{-1} are fast enough to destroy molecules (Hollenbach and McKee 1980). Such shock velocities may result from the outflow of material from young stellar objects, from stellar winds, or from supernova explosions. Clearly, dissociative shocks are intimately associated with stars: they may be generated during the birth, throughout the life, and by the explosive death of stars. Emission from fast shocks may serve as a tracer of active star formation in the Galaxy.

In *dissociative* shocks the slowly cooling shocked gas may be treated to good approximation as a single fluid which has undergone a discontinuous change in temperature and density at the shock front. Draine (1980) has termed "J"-type those shocks in which an effectively discontinuous *jump* in the fluid variables occurs. The physical processes leading eventually to the reformation of molecules in dissociative J-type shocks have been discussed by Hollenbach and McKee (1979), and the emission line strengths predicted for transitions of certain atomic and molecular species have been presented by McKee, Chernoff, and Hollenbach (1984).

Chernoff, Hollenbach, and McKee (1982) have suggested that in addition to the C-type shock that gives rise to the H_2 $v = 1 \rightarrow 0$ and high-J CO emission in Orion-KL, a faster J-shock may be present where an outflow that drives the C-shock impacts a shell of swept-up material. Haas, Hollenbach, and Erickson (1986) have argued that their observation of the 35 μm line of [Si II] is evidence of the ionization produced by such a shock, and McKee and Hollenbach (1987) have suggested that observations of the H51α recombination line of hydrogen (Hasegawa and Akabane 1984) lend further support to the two-shock picture.

In the present paper we treat the structure of dissociative J-type shocks with particular attention to chemical processes, including the photochemical effects of the ultraviolet radiation field that is generated in the hottest part of the shocked gas region. We expand the network of chemical reactions that was adopted by Hollenbach and McKee (1979) to include molecules of the elements nitrogen, sulphur, and silicon, as well as complex hydrocarbon species containing up to three carbon atoms, and we show how the abundances of the various molecular species vary through the shocked region. The silicon chemistry, in particular, is directly relevant to any discussion of the strength of the 35 μm [Si II] line.

We include the effects of the conversion of Lyα photons into radiation of the two-photon continuum and into H_2 Lyman band emission lines (Neufeld and McKee 1989). We also present a new treatment of the photodissociation of the important CO molecule in fast shocks, a treatment made possible by recent laboratory measurements of CO line absorption that have been made by Letzelter *et al.* (1987) and by Yoshino *et al.* (1988).

We review the physical processes that govern the structure of the cooling gas behind a fast dissociative shock, and we discuss the chemical processes that lead to the reformation of molecules and their subsequent evolution. We present our results for the column densities of the different molecules that are generated in the warm, shocked region, and we discuss their dependence on the shock parameters. We have determined the structure of shocks of velocity 60, 80, 90, and 100 km s^{-1} in gas of preshock density 10^4, 10^5, and 10^6 cm^{-3}.

II. PHYSICAL PROCESSES IN THE SHOCKED GAS

a) Structure of Fast Molecular Shocks

Fast shocks in molecular gas may be conveniently divided into three distinct regions: (i) a radiative precursor in which supersonic gas flowing into the shock is heated, dissociated, and ionized by photons emitted by downstream hot shocked gas; (ii) a thin adiabatic shock front in which collisions or plasma instabilities compress and heat the gas; and (iii) a thicker postshock region where the now subsonic gas cools by the emission of line and continuum radiation. In the first region, radiation is converted into thermal energy and into chemical potential energy; in the second, energy of bulk motion is converted into thermal energy with a consequent increase in entropy; and in the third, thermal energy is converted to radiation, and the shocked gas cools, ions recombine, and molecules reform. The present paper deals with the problem of determining the structure of the third region.

We treat the problem in plane-parallel geometry and under the assumption that there exists a frame in which the local time derivative of every variable is zero. This second assumption of "steady state" is appropriate to those shocks which evolve on a time scale much longer than the time taken for material to pass through them. Our treatment is restricted to shocks fast enough that the ions, electrons, and neutrals remain coupled as a single fluid despite the fact that the magnetic field is frozen to the charged particles alone. With the magnetic fields present in the interstellar medium, this restriction requires a shock velocity of at least 50 km s^{-1}, enough to dissociate all molecules as they pass through the shock and thereby to increase the cooling time in the shocked gas beyond the ion-neutral collision time scale. Any magnetic field is assumed to lie in the plane of the shock front.

Given these restrictions, the equations of mass, momentum, and energy conservation which govern the hydrodynamics may be written (Field *et al.* 1968):

$$\rho v = \rho_0 v_0 , \tag{1}$$

$$p + \rho v^2 + B^2/8\pi = p_0 + \rho_0 v_0^2 + B_0^2/8\pi , \tag{2}$$

$$\frac{d}{dz} v(\rho v^2/2 + p + u + B^2/4\pi) = -\Lambda , \tag{3}$$

where ρ is the mass density, v is the fluid velocity, p is the pressure, B is the magnetic field, u is the internal energy density of the fluid, z is the distance behind the shock front, Λ is the net cooling rate per unit volume, and the subscript 0 following any variable indicates a preshock value.

The internal energy density u includes the energy associated with translational thermal motion and that deriving from excitation of rotational and vibrational modes of molecular hydrogen:

$$u = \tfrac{3}{2}p + n(H_2) \sum (E_i f_i) , \tag{4}$$

where $n(H_2)$ is the number density of H_2 molecules, and E_i and f_i are the excitation energy and fractional population of the ith H_2 rovibrational level. The thermal pressure p is given by the ideal gas law:

$$p = \frac{\rho k T}{\mu} , \tag{5}$$

where μ is the mean particle mass. The magnetic field is frozen to the charged particles, which are assumed to remain coupled to the fluid as a whole. The B-field perpendicular to the shock direction is therefore given by

$$Bv = B_0 v_0 . \tag{6}$$

Equations (1)–(3) are obeyed not only in the postshock region but also across the adiabatic shock front if Λ is set equal to zero. These equations therefore govern the jump conditions. For a strong shock ($\rho_0 v_0^2 \gg p_0 + B_0^2/8\pi$) in fully ionized gas, the jump conditions lead to an initial postshock temperature of

$$T_{ps} = 13.8 v_s^2 \text{ K} , \tag{7}$$

where $v_s = v_0/10^5$ cm s^{-1} is the shock velocity in km s^{-1}. As the gas cools, the density increases so as to preserve the initial momentum flux given on the right-hand side of equation (2). However, because the magnetic contribution to the total momentum flux, $B^2/8\pi$, increases monotonically with density under the conditions of flux freezing, the allowed density increase is limited by the requirement that $B^2/8\pi < p_0 + \rho_0 v_0^2 + B_0^2/8\pi$. In a strong shock the compression is therefore limited to

$$x_{max} = \frac{\rho_{max}}{\rho_0} = \sqrt{\frac{8\pi\rho_0 v_0^2}{B_0^2}} = 0.77 v_s \sqrt{\frac{n_0}{\text{cm}^{-3}} \left(\frac{\mu G}{B_0}\right)^2} , \tag{8}$$

where n_0 is the preshock density of hydrogen nuclei.

The cooling time scale at any point in the shock may be defined as

$$t_{\rm cool} = \frac{u+p}{\Lambda} \sim \frac{5nkT}{2\Lambda},$$

where n is the local density of hydrogen nuclei, while the time scale for a chemical process with rate coefficient, k, may be defined

$$t_{\rm chem} = \frac{1}{knA},$$

where A is the abundance of the reaction partner relative to hydrogen nuclei. If cooling takes place by excitation of atomic or molecular transitions that are not significantly collisionally de-excited, the volume cooling rate Λ is proportional to n^2, and both time scales have a $1/n$ dependence. This behavior suggests that the total column density of hydrogen nuclei,

$$N_{\rm H} = \int_0^z n(z')dz',$$

may be useful as a coordinate in measuring distances behind the shock front. Noting that $d/dt = (n_0 v_0)d/dN_{\rm H}$, we may write the cooling and chemical time scales in terms of the new coordinate $N_{\rm H}$:

$$N_{\rm cool} = \frac{5kT}{2}\frac{n^2}{\Lambda}\frac{v_0}{x}, \qquad N_{\rm chem} = \frac{v_0}{kxA}, \tag{9}$$

where $x = n/n_0$ is the compression.

If the interstellar magnetic field strength increases with the preshock density as $n_0^{1/2}$, the maximum compression given in equation (8) is independent of n_0. The column densities corresponding to the cooling and chemical time scales given in equation (9) are therefore also independent of preshock density, except insofar as collisional de-excitation effects may lead Λ to increase less rapidly than n^2. Indeed, were it not for such effects, the shock structure, expressed in terms of the coordinate $N_{\rm H}$, would be entirely independent of n_0.

Because the abundances of particular molecules, atoms, and ions determine the total cooling rate, the hydrodynamic equations given above must be integrated simultaneously with a coupled set of differential equations governing the chemical evolution of the shocked gas. The chemical network must reproduce accurately the abundances of the major coolant species. The shocked gas region can be subdivided to good approximation into two distinct parts: a hotter region containing atoms, and singly and multiply charged ions but no molecules, and a cooler region containing atoms, only singly charged ions, and molecules. The dividing line between the two regions occurs at a temperature of $\sim 10^4$ K.

Elaborate computer models have been designed to study fast shocks in atomic gas such as those which give rise to emission from supernova remnants and Herbig-Haro objects (Shull and McKee 1979; Raymond 1979; Binette, Dopita, and Tuohy 1985). In the present treatment of molecular shocks, the atomic shock code of Raymond has been used to follow the gas down to a temperature of 10^4 K. The integration is then taken up by our molecular shock computer model which accepts as a boundary condition an initial ionization state and incident radiation field produced in the gas above 10^4 K. Ultraviolet radiation produced in the hot atomic region has a profound effect on the ionization state and chemical evolution in the cool downstream molecular region.

In making use of an atomic shock model to follow the initial phase of cooling in the shocked region, we make the implicit assumption that the preshock gas is atomic. In the case of fast shocks the radiation field may be sufficient to preionize, preheat, and predissociate the gas entering the shock, validating this assumption, and even if it were not and the preshock gas were molecular, the gas would rapidly be dissociated immediately after passing through the shock front. For shock velocities ≥ 60 km s^{-1} a negligible fraction of the incident bulk kinetic energy would be used up in dissociating even a purely molecular preshock medium (McKee and Hollenbach 1987).

b) Heating and Cooling

Gas in the shocked region cools mainly by excitation of excited electronic levels of atoms and atomic ions and of rovibrational levels of molecules. Gas is heated by absorption of radiation emitted by warmer upstream gas, and by the release of chemical energy to the gas when molecules are formed. Recombination of atoms, by contrast, releases chemical potential energy directly into the radiation field as recombination lines and continua rather than into the gas. Only the formation of the most abundant molecule, molecular hydrogen, results in a significant heating of the gas.

In the region where the gas temperature is greater than 3000 K, excitation of forbidden, semiforbidden, and allowed transitions of atoms and atomic ions is the major cooling process. Above 10^4 K the cooling of the shocked gas is followed using the computer program of Raymond, which includes as possible coolants all the important ionization states of the elements H, He, C, N, O, Ne, Mg, Si, S, Ar, Ca, and Fe. Below 10^4 K, only the following atoms and atomic ions are included in the cooling calculation: H, He, C, C^+, N, N^+, O, O^+, Mg^+, Si^+, S^+, and Fe^+. The level populations in each ion are calculated by solving the equations of statistical equilibrium for a 2, 5, or 13 state system. The collisional excitation rates and spontaneous radiative probabilities for the relevant transitions have been compiled by Mendoza (1983).

Because the present study is concerned with shocks with preshock densities of 10^4 cm^{-3} and greater, many of the transitions that are important coolants in shocks of lower density are quenched by collisional de-excitation. Allowed transitions, therefore, in particular those of the ions S^+ and Mg^+, assume a greater importance than in the lower density shocks used to model supernova remnants.

Below 5000 K, rotational transitions of OH, CO, H_2O, and rovibrational transitions of H_2 contribute significantly to the cooling. For the molecules OH and CO we have used the "universal cooling function" of Hollenbach and McKee (1979). In calculating the cooling due to CO, we have used the critical density recommended by McKee *et al.* (1982). For OH, the universal cooling function was tested at low optical depth and low density against statistical equilibrium calculations carried out with G. Melnick (using the collision rates adopted by Melnick, Genzel, and Lugten 1987). Results of the two calculations are in remarkable agreement and call for no change in the critical density given by Hollenbach and McKee (1979). H_2O cooling is fitted less well by the Hollenbach and McKee formalism because the polyatomic water molecule does not have a simple energy level structure. We adopt instead the general cooling function derived by Neufeld and Melnick (1987).

Molecular hydrogen cooling is calculated at each point in the shock by solving the equations of statistical equilibrium for the H_2 level populations. Because only quadrupole-allowed transitions with small Einstein A-values contribute to the cooling, optical depth effects are unimportant. At temperatures above ~ 500 K, we use the H_2 collisional rate coefficients adopted by Hollenbach and McKee (1979) and by Draine, Roberge, and Dalgarno (1983). For a largely atomic gas these rate coefficients imply a critical density for de-excitation of vibrational states of $n_{cr}(H_2) = 6 \times 10^4 T_2^{-1/2}$ cm^{-3} (Hollenbach and McKee 1979), where $100T_2$ K is the temperature. Because the density in the postshock region is at least 5×10^5 cm^{-3} in all the cases we consider, the H_2 level populations are always close to LTE for $T \geq 500$ K. At lower temperatures, the rate coefficients may be reduced by the presence of an energy barrier. Unpublished collisional cross sections calculated by Chu lead Hollenbach and McKee (1979) to conclude that the expression given above for $n_{cr}(H_2)$ must be multiplied by the factor $\exp[(400/T)^2]$. The presence of such an energy barrier must be regarded as uncertain, however, and collisionally excited rovibrational transitions of large ΔJ but small ΔE (Buch and Dalgarno 1989), if rapid, may in any case partly offset the resulting increase in $n_{cr}(H_2)$.

Gas at each point in the postshock region is subject to heating by radiation emitted by hotter upstream gas. If the mean intensity of the radiation is J_ν, then the heating associated with a photoionization or photodissociation process of cross section σ_ν is given by

$$-\Lambda_{\rm photo} = 4\pi n(\mathrm{X}) \int J_\nu \sigma_\nu \frac{(\nu - \nu_0}{\nu_0} d\nu ,$$

where $-\Lambda_{\rm photo}$ is the heating rate per unit volume, $n(\mathrm{X})$ is the number density of reactant particles, and $h\nu_0$ is the energy difference between the reactant and the products of the photoreaction.

Formation of molecules in exothermic chemical reactions can affect the energy balance of the shocked gas. Below a temperature of ~ 1000 K, formation of molecular hydrogen takes place primarily on the surfaces of grains. Each time a molecule is formed, the associated heat of formation, 4.48 eV, is divided between rovibrational and kinetic energy of the ejected molecule and thermal energy of the grain that catalyzed the reaction. If the gas density exceeds the critical density $n_{cr}(H_2)$, H_2 molecules produced in excited rovibrational states will transfer almost all of their excitation energy to thermal energy of the gas by means of collisional de-excitation. In one model for the formation of H_2 on grain surfaces (Duley and Williams 1986), 0.4 eV of the heat of formation is transferred to the grain, the remainder serving to heat the gas and to excite rovibrational states. Thus for $n \gg n_{cr}(H_2)$ the heating associated with this process is given by

$$-\Lambda_{H_2} = (4.08 \text{ eV}) k_{H_2} n n(\mathrm{H}) , \tag{10}$$

where k_{H_2} is the effective rate coefficient for the grain formation process.

Gas phase reactions involving the intermediates H^- and H_2^+ only contribute to H_2 formation and the associated heating when the temperature is above 1000 K. At such a temperature, atomic and molecular cooling processes are efficient enough to render heating from H_2 formation of negligible importance; heating associated with gas phase reaction routes to molecular hydrogen is therefore neglected. Other exothermic gas phase reactions involving molecules of the heavy elements are similarly negligible sources of heating, the abundance of the reactants being far lower.

The hydrogen recombination cooling is given by

$$\Lambda_{\rm rec} = \sum_n 4\pi \int j_\nu^n \frac{(\nu - \nu_n)}{\nu_n} d\nu , \tag{11}$$

where j_ν^n is the continuum volume emissivity resulting from recombination to the level of principal quantum number n, and ν_n is the frequency of the corresponding continuum edge.

Inelastic collisions between gas particles and grains may result in a transfer of energy from gas to grains. The mean energy transfer per collision may be represented (Burke and Hollenbach 1983) by the expression: $E = 2kT\alpha$, where the accommodation coefficient α is of order—but necessarily less than—unity. The ratio of gas-grain cooling to H_2 formation heating is given by

$$\frac{2kT\alpha}{4.08 f_{\rm gr} \text{ eV}} = 0.04 \left(\frac{T}{1000 \text{ K}} \right) \frac{\alpha}{f_{\rm gr}} , \tag{12}$$

where $f_{\rm gr}$ is the probability that a gas-grain collision is followed by H_2 formation. Thus unless $f_{\rm gr}$ is small the gas-grain cooling rate is much smaller than the H_2 formation heating rate at temperatures at which either process is important. For the reasons given in § IV*a* below, we assume that $f_{\rm gr}$ is close to unity for grains of radius $a \geq 100$ Å. Given that assumption we may neglect gas-grain cooling, even if there is a substantial abundance of smaller grains (10 Å $< a <$ 100 Å) for which α is large but $f_{\rm gr}$ is small.

c) Radiative Transfer

In plane-parallel geometry, the mean intensity is given by

$$J_\nu(\tau_\nu) = \tfrac{1}{2}\int_0^\infty S_\nu E_1(|\tau'_\nu - \tau_\nu|)d\tau'_\nu = \tfrac{1}{2}\int_0^\infty j_\nu E_1(|\tau'_\nu(z) - \tau_\nu|)dz\ , \tag{13}$$

where S_ν is the source function, j_ν is the volume emissivity, τ_ν is the monochromatic optical depth to the boundary, z is the distance into the shocked region, and $E_1(\tau)$ is the exponential integral function, defined as

$$E_1(\tau) = \int_1^\infty \frac{\exp(-\tau\mu)}{\mu}\,d\mu\ . \tag{14}$$

Although the function $E_1(\tau)$ diverges at the origin, the divergence is logarithmic, so the integrals given in equation (13) are well-defined. However, the value of E_1 is often limited to some maximum $E_{1,\max}$ in shock calculations to take account approximately of departures from plane-parallel geometry (Shull and McKee 1979; Raymond 1979). The integration variable μ in equation (14) represents the secant of the angle between the normal to the shock front and each ray which contributes to the overall mean intensity. If the shocked region, instead of being a plane-parallel slab, is in reality a thin spherical shell of thickness t and radius R, rays incident at a given point from other parts of the shocked region will, on average, have a maximum μ of order $(R/t)^{1/2}$. Account can be taken of this finite maximum obliquity by replacing the upper limit on the integral in equation (13) by $(R/t)^{1/2}$. This is approximately equivalent to replacing $E_1(\tau)$ by min $[E_1(\tau), E_{1,\max}]$, where $E_{1,\max} = \ln(R/t)/2$. We follow Hollenbach and McKee (1979) in adopting $E_{1,\max} = 3$, corresponding to $R/t \sim 400$.

The optical depth τ_ν is given by

$$\int_0^z \kappa_\nu\,dz'\ ,$$

where κ_ν is the continuum opacity resulting from all photoionization and photodissociation processes as well as from dust absorption. Following Hollenbach and McKee (1979), we take the absorptive part of the dust opacity as 5×10^{-22} cm$^2 n$, independent of frequency. The appropriate value for the dust opacity is rather uncertain, and depends upon the conditions in the preshock gas and the effects of the shock in destroying and fragmenting grains.

i) *The Volume Emissivity, j_ν*

Line and continuum emission processes following both recombination and excitation contribute to the emission from the shocked region. Collisionally excited line emission from atomic ions and neutral atoms is computed using the solution to the equations of statistical equilibrium obtained for the purpose of calculating the total cooling. The emissivity in each line is given by

$$\int j_\nu\,dv = \frac{n(\mathrm{X}) f_u A_{ul} E_{ul}}{4\pi}\ , \tag{15}$$

where n(X) is the density of the emitting species, A_{ul} is the spontaneous radiative rate for the transition, f_u is the fractional population in the upper level, and E_{ul} is the transition energy. Except for the Lyα resonance line, considered separately below, we ignore line optical depth effects in determining the downstream flux of photodestructive UV radiation.

Recombination of hydrogen and helium results in both line and continuum emission (see Osterbrock 1974). Helium recombination to triplet states is followed by cascading to the 2 ^3S level, which either decays to the ground state by a spin-forbidden transition with probability 1.13×10^{-4} s^{-1}, or is collisionally excited to 2 ^1S or 2 ^1P. The collisional process dominates at densities above 3000 cm^{-3}. The 2 ^1P state decays to the 1 ^1S ground state by a dipole-allowed transition with the emission of a photon at 58.4 nm, while the 2 ^1S state undergoes a two-quantum decay resulting in a broad continuum peaked (in number per unit energy interval) at 10.3 eV, one-half the transition energy (Drake, Victor, and Dalgarno 1969). At densities above 10^8 cm^{-3}, collisional excitation from 2 ^1S to 2 ^1P reduces the strength of the two-photon continuum. The 2 ^1S and 2 ^1P states are populated by collisionally induced transitions from 2 ^3S, and by cascade following recombination into excited singlet states.

The 58.4 nm photons slightly increase the ionization fraction of hydrogen. The two-photon continuum is of far greater importance because it provides a source of radiation longward of the Lyman limit, where molecules are vulnerable to photodestruction. Indeed, at shock velocities below 100 km s^{-1}, photodissociation of CO by the helium two-photon continuum is the main destruction process in that molecule, with significant consequences for the entire chemistry of carbon-bearing species. All the other strong recombination lines and continua of helium fall at energies below 5 eV, an energy region in which hydrogen Balmer lines and continua dominate the emissivity, and we may omit the contribution from helium recombination at these lower energies.

ii) *Transfer of Lyα Radiation*

After their original emission in recombining gas at temperatures above 6000 K, Lyα photons are resonantly scattered a large number of times by ground-state hydrogen atoms before arriving in downstream molecular gas where their photodestructive effects are felt. The path length that such photons travel, on average, is consequently increased by a factor of 10 or more (Adams 1975; Hummer and Kunasz 1980), and they suffer a greater attenuation by dust absorption than photons which are not resonantly scattered.

Because between 40% and 90% of the energy of bulk motion that enters a fast molecular shock is radiated in the Lyα line, the details of its transfer are of considerable importance. We have adopted the approximate, analytic treatment of Neufeld and McKee (1989), which includes the effects of dust absorption, of the pumping of H_2 Lyman band emission lines, and of the conversion of Lyα photons to radiation of the two-photon continuum following collisionally induced transitions from the resonantly excited H(2p)

state to the metastable H(2*s*) state. Our treatment implicitly assumes the presence of preshock hydrogen atoms, with a column density of at least 10^{20} cm^{-2}. Much of the Lyα radiation produced in fast molecular shocks is absorbed by the nearly coincident H_2 *B–X* 1–2 *P*(5) and 1–2 *R*(6) lines and is converted into H_2 Lyman band emission before it can be absorbed by dust. This process heats the gas and modifies the ultraviolet radiation field in the downstream molecular region. In the present calculations we neglect radiative transfer effects resulting from the presence of a velocity discontinuity at the shock front.

d) Computational Method

The coupled set of differential equations governing the chemical evolution of the molecular gas is stiff in the sense of having normal modes which decay at a wide range of different rates. They are integrated using the GEAR algorithm (Gear 1971), a predictor-corrector scheme with a variable step size for which a well-tested computer program has been written and is widely used. After each integration of the chemical equations, the hydrodynamic variables are updated and the emission spectrum from the current step is calculated. The radiation flux which determines the photochemistry and heating at the next step is then calculated by integrating equation (13) over all *previous* steps. Radiation from downstream gas (whose properties are yet to be calculated) is therefore neglected, an approximation which is expected to be good because the temperature of the gas and therefore of the radiation it emits is decreasing monotonically. Most of the radiation that is hard enough to destroy molecules is produced by recombination of hydrogen, which takes place before significant molecule formation has occurred.

III. PHOTODISSOCIATION AND PHOTOIONIZATION

After the shocked gas has cooled below a temperature of $\sim 10^4$ K, reformation of molecular hydrogen begins by means of chemical processes both in the gas phase and on grain surfaces. Molecules containing the heavy elements are then formed via a complex network of gas phase chemical reactions and radiative processes which take place under the influence of an ultraviolet radiation field. Table 1 shows how the character of the radiation field depends upon the shock velocity.

If the entire bulk energy input to the shock were radiated as photons of mean energy 10 eV, the cooler molecular region would be subject to a photon flux of

$$\frac{(\rho_0 v_0^3/4)}{10\ \mathrm{eV}} \sim 3 \times 10^7 \left(\frac{v}{100\ \mathrm{km\ s^{-1}}}\right)^3 \left(\frac{n_0}{\mathrm{cm^{-3}}}\right) \mathrm{photons\ cm^{-2}\ s^{-1}}\ .$$

The resultant photoionization or photodissociation rate would be

$$\sim 3 \times 10^{-10} \left(\frac{v}{100\ \mathrm{km\ s^{-1}}}\right)^3 \left(\frac{n_0}{\mathrm{cm^{-3}}}\right) \left(\frac{\sigma}{10^{-17}\ \mathrm{cm^2}}\right) \mathrm{s^{-1}}\ . \tag{16}$$

Except for those molecular ions which undergo rapid dissociative recombination, the rates (16) often exceed the destruction rates due to chemical processes.

In Figure 1 we show the effective radiation field at various points in the shocked gas region, each identified by its column density behind the shock front.

The photodissociation or photoionization rates are given by

$$r_{h\nu} = \int \frac{4\pi J_\nu \sigma_\nu}{h\nu}\, d\nu\ , \tag{17}$$

where σ_ν is the corresponding cross section at frequency ν. We evaluate the above integral on a grid of frequencies separated in energy by 0.5 eV below 20 eV and by 2 eV between 20 and 80 eV. The spectrum of the photodestructive radiation is dominated by a few strong lines, in particular Lyα, lines of the H_2 Lyman band systems, and, for shock velocities above 80 km s^{-1}, a line of C III at 97.7 nm. The cross section data were taken from van Dishoeck (1987) and the various sources listed by Neufeld (1987). With the exception of the molecules H_2, N_2, and CO, photodissociation cross sections vary slowly over energy intervals of 0.5 eV, so in evaluating the photodissociation rate we may take an average of the cross section throughout the energy range of each bin. Photoionization cross sections show an even slower variation with energy. Because of the great strength of the Lyα and C III 97.7 nm lines, however, we use the cross sections at the precise line energies in place of the averages over the energy bins that contain them.

a) Photodissociation of CO

Photodissociation of CO requires special treatment. No continuum absorption by CO has been detected longward of the Lyman limit. Photodissociation takes place at wavelengths shortward of 107.6 nm by means of line absorption to one of several predisso-

TABLE 1

CHARACTER OF THE RADIATION FIELD WHEN $T = 10^4$ K: PERCENTAGE OF THE INTENSITY CARRIED IN DIFFERENT ENERGY BINS

Shock Velocity (km s^{-1})	< 10.2 eV	Lyα	10.2–13.6 eV	> 13.6 eV
60	1.4	97.2	0.2	1.3
80	2.0	93.9	0.4	3.7
90	12.7	60.0	7.6	19.7
100	7.5	29.3	13.9	49.4

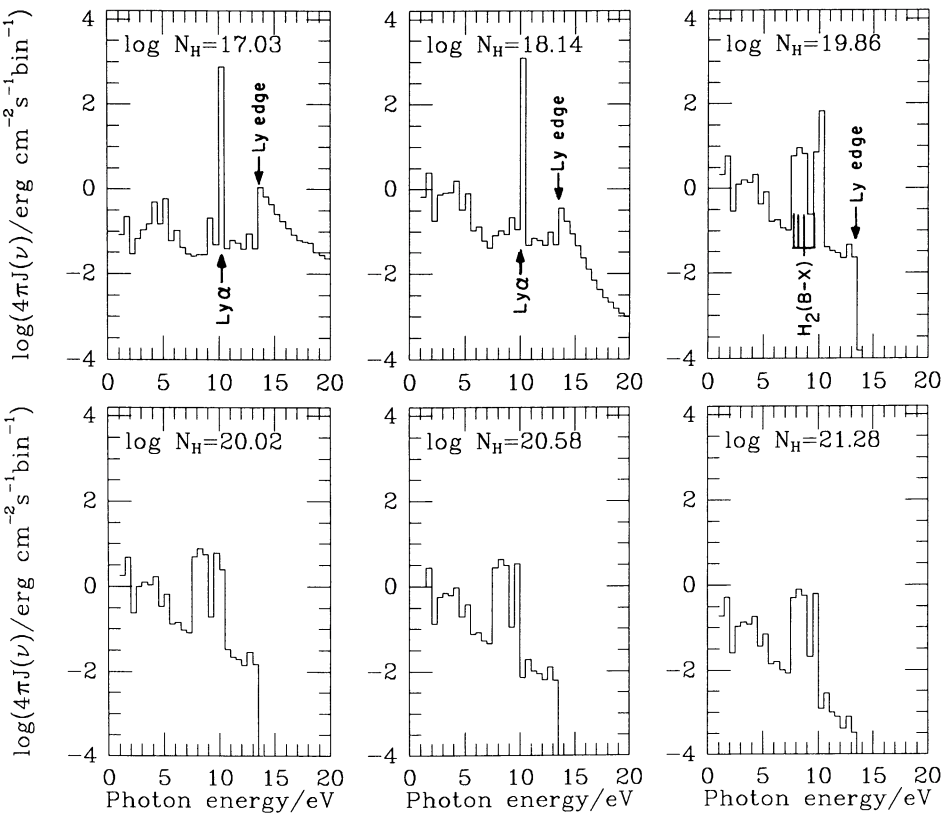

FIG. 1.—Radiation field at various points in the shocked gas

ciated electronically excited states followed by a radiationless transition to a repulsive state. The probability of dissociation following line absorption, η, is usually close to unity for those states which are significantly predissociated.

Lists of photodissociating transitions has been compiled by van Dishoeck and Black (1987, private communication) and by Viala *et al.* (1988), who give predissociation probabilities based on the experimental absorption spectra of Letzelter *et al.* (1987) and Yoshino *et al.* (1988). Oscillator strengths and cross sections are tabulated by Yoshino *et al.* (1988) and by Viala *et al.* (1988).

The absorption lines that lead to dissociation have substantial natural line widths that may be written

$$\frac{\Delta v}{\text{km s}^{-1}} = \frac{1}{4\pi}\left(\frac{\lambda}{100\text{ nm}}\right)\left(\frac{A_{\text{tot}}}{10^{10}\text{ s}^{-1}}\right), \tag{18}$$

where λ is the line wavelength and A_{tot} is the total decay rate of the pumped level as a result of both predissociation and radiative decay back to the ground state. The natural widths are often broader than the thermal Doppler width at the temperatures at which CO is formed.

Continuum radiation capable of photodissociating CO is produced predominantly by the two-photon decay of metastable He(2 ^1S) atoms. The production of the He two-photon continuum takes place in the region of singly ionized helium and has been discussed in § II*c*.

We consider a thin slab of which emits He(2 ^1S–1 ^1S) photons at a rate s (measured in photons cm^{-2} s^{-1} sr^{-1}). The rate of CO photodissociation at a downstream point P resulting from absorption in a single isolated line is given by

$$r_{\text{pd}} = 2\pi s\eta \int \Phi_\nu \sigma_\nu E_1(\tau_\nu) d\nu\ , \tag{19}$$

where Φ_ν is the normalized frequency distribution of the two-photon radiation, σ_ν is the CO line absorption cross section, and τ_ν is the optical depth for a ray normal to the slab. The absorption cross section per CO molecule, σ_ν, may be written

$$\sigma_\nu = \frac{f n_J}{\nu_0}\frac{\pi e^2}{m\Delta v}\phi_x\ , \tag{20}$$

where f is the oscillator strength, n_J is the fractional population in the lower level of the absorbing transition, ν_0 is the line center frequency, and ϕ_x is the normalized CO line profile expressed as a function of $x = (\nu - \nu_0)/\Delta\nu$, where $\Delta\nu$ is the line width. Assuming that the line profile, ϕ_x, and level population, n_J, remain constant throughout the medium, we may express the optical depth τ_ν as

$$\tau_\nu = N_{\text{CO}}\sigma_\nu + \tau_c\ , \tag{21}$$

where N_{CO} is the carbon monoxide column density out to point P, and τ_c is the continuum optical depth. Neglecting the variation of Φ_ν over the line profile, we may write the photodissociation rate in a single isolated line as

$$r_{pd} = 2\pi s \eta \Phi_\nu(\nu_0) f n_J \frac{\pi e^2}{mc} F(\tau_0, \tau_c) , \tag{22}$$

where τ_0 is the integrated optical depth in the line:

$$\tau_0 = \frac{f n_J}{\nu_0} \frac{\pi e^2}{m \Delta v} N_{CO} , \tag{23}$$

and

$$F(\tau_0, \tau_c) = \int \phi_x E_1(\phi_x \tau_0 + \tau_c) dx , \tag{24}$$

In the limit of large τ_0, the Lorentz wings dominate the profile and ϕ_x may be approximated by

$$\phi_x = \frac{1}{\pi(1 + x^2)} .$$

For $\tau_0 \gg 1$ we may then write

$$F(\tau_0, \tau_c) = \int \frac{1}{\pi(1 + x^2)} E_1\left[\frac{\tau_0}{\pi(1 + x^2)} + \tau_c\right] dx = \int_0^1 \frac{d\mu}{\mu} \int_{-\infty}^{+\infty} \frac{1}{\pi(1 + x^2)} \exp\left[-\tau_0/\pi(1 + x^2)\mu\right] \exp\left(-\tau_c/\mu\right) dx$$

$$\approx \int_0^1 \frac{d\mu}{\mu} \int_{-\infty}^{+\infty} \frac{1}{\pi x^2} \exp\left(-\tau_0/\pi x^2 \mu\right) \exp\left(-\tau_c/\mu\right) dx = \int_0^1 \frac{d\mu}{\mu} \sqrt{\frac{\mu}{\tau_0}} \exp\left(-\tau_c/\mu\right) = \frac{E_{3/2}(\tau_c)}{\sqrt{\tau_0}} ,$$

where

$$E_{3/2}(\tau_c) = \int_1^\infty y^{-3/2} e^{-\tau_c y} dy . \tag{25}$$

As τ_0 tends to zero, $F(\tau_0, \tau_c)$ diverges logarithmically, although we limit its value to 3 in accordance with our earlier discussion of radiative transfer in § IIc. We fit the limiting behavior of F at high and low τ_0 by adopting the following approximate expression:

$$F(\tau_0, \tau_c) = \frac{E_{3/2}(\tau_c)}{(2/3) + \sqrt{\tau_0}} . \tag{26}$$

The total CO dissociation rate may then be obtained by summing equation (22) over every absorption line in each absorption band:

$$R_{pd}(N_{CO}, \tau_c) = 2\pi s \sum_{\text{bands}} \sum_{\text{lines}} \eta \Phi_\nu f n_J \frac{\pi e^2}{mc} F\left(\frac{f n_J}{\nu_0} \frac{\pi e^2}{m \Delta v} N_{CO}, \tau_c\right) . \tag{27}$$

At high optical depths line overlap effects become important. The pumping rate of a given line can only continue to decline as $\tau_0^{-1/2}$ when the optical depth at the midpoint between neighboring absorption lines is small. Once the midpoint optical depth becomes large, pumping can no longer continue to take place further and further out in the Lorentz wings, and the photodissociation rate starts to fall exponentially. We take approximate account of such effects by multiplying the function F by an exponential factor $\exp(-\tau_m)$, where τ_m, the midpoint optical depth, is related to the frequency spacing between adjacent lines, ν_{sep}, by the expression

$$\tau_m = \frac{\tau_0}{\pi[1 + (\nu_{sep}/\Delta v)^2]} . \tag{28}$$

For absorption lines in an R- or P-branch the frequency spacing, to first order, is equal to $2Bc$, where B is the rotational constant and c is the velocity of light. For lines in a Q-branch the spacing is very variable and depends on the difference between the B and D rotational constants in the upper and lower states. We make the further approximation of taking $\nu_{sep} = 2Bc$. Then the rate of photodissociation of CO by the two-photon He($2\,^1S \rightarrow 1\,^1S$) continuum is given by

$$R_{pd}(N_{CO}, \tau_c) = 2\pi s E_{3/2}(\tau_c) \frac{\pi e^2}{mc} \sum_{\text{bands}} \sum_{\text{lines}} \eta \frac{f n_J}{(2/3) + \sqrt{\tau_0}} \Phi_\nu \exp\left\{-\frac{\tau_0}{[1 + (2Bc/\Delta v)^2]}\right\} . \tag{29}$$

In Figure 2 we plot $R_{pd}/2\pi s$ as a function of the carbon monoxide column density for the case of zero continuum optical depth, τ_c. The quantity $R_{pd}/2\pi s$ may be regarded as an effective CO photodissociation cross section for an average photon in the He($2\,^1S \rightarrow 1\,^1S$) continuum, and has been calculated for the level populations n_J obtained in LTE at 1000 K. The temperature dependence of R_{pd} is very weak, and we neglect it in our computations of the CO abundance in the shocked gas region.

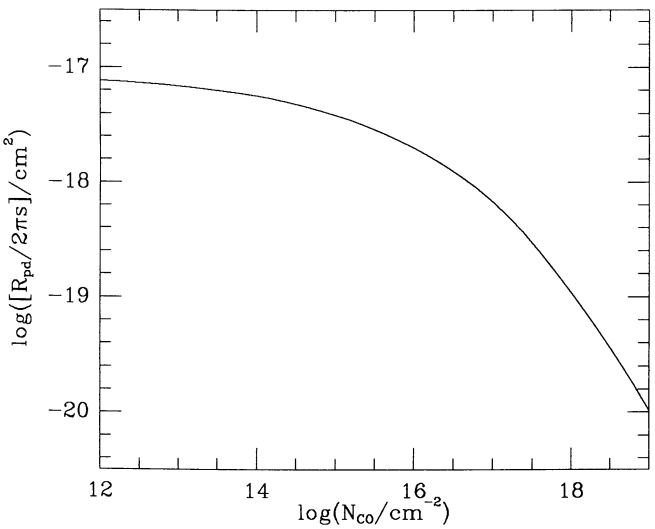

FIG. 2.—CO photodissociation rate per unit flux of He(2 ^1S–1 ^1S) photons, as a function of the shielding CO column density.

Coincidences between emission lines of atomic ions in the hot part of the shocked gas region and photodissociating transitions in CO may, in principle, enhance the photodissociation rate. We find one coincidence involving a strong atomic emission line: the 98.9790 nm line of N III is found to overlap several lines of the CO ($X\ ^1\Sigma \rightarrow G\ ^1\Pi$) Q-branch. However, the resulting enhancement in the photodissociation rate is negligible for the shock velocities of present interest, because the N III emission line is only significantly excited when the shock velocity exceeds 90 km s^{-1} and is attenuated as a result of absorption by the coincident 1–0 $Q(3)$ line of the H_2 Werner band.

IV. CHEMICAL PROCESSES

After the gas behind a dissociative shock front has cooled below $\sim 10^4$ K, atoms begin to associate and form molecules. To describe the chemistry in the cooling gas, we have included 285 chemical reactions and 55 radiative processes involving 80 species, using data compiled from the lists of Herbst (1983), Mitchell (1984), Anicich and Huntress (1986), Millar *et al.* (1986), and Pineau des Forets *et al.* (1986, 1987). A complete listing is given by Neufeld (1987). Where information is available, we have taken into account modifications due to nonthermal populations (Wagner and Graff 1987; Graff and Dalgarno 1987). In extrapolating to higher temperatures, we have adopted the view of Leen and Graff (1988) and have assumed a constant rate coefficient at temperatures above 300 K except where explicit data are available.

a) Formation of H_2

In gas with a significant ionization fraction, H_2 is formed by the sequence

$$H + e \rightarrow H^- + h\nu\ ,$$

$$H^- + H \rightarrow H_2 + e\ .$$

The H^- intermediate may undergo mutual neutralization with H^+,

$$H^- + H^+ \rightarrow H + H\ ,$$

a reaction which limits the efficiency of H_2 formation (Dalgarno and McCray 1972).

Once the ionization fraction in the shocked gas falls below 2%, the effectiveness of the gas phase scheme diminishes rapidly and grain surface reactions come into play. If H_2 formation takes place only on grains of radius $a \geq 100$ Å, standard grain abundances (Mathis, Rumpl, and Nordsieck 1977) yield a formation rate

$$k_{gc} = 3 \times 10^{-18} T^{1/2} n f_{gr}\ \text{s}^{-1}\ ,$$

where f_{gr} is the fraction of collisions that result in H_2 formation. The H_2 abundances observed suggest that $f_{gr} \sim 1$ under the conditions present in cold, diffuse interstellar clouds (Jura 1974). However, the efficiency of H_2 formation is uncertain at the higher grain temperatures ($T \sim 100$ K) and gas temperatures ($T \sim 1000$ K) achieved in the molecular gas behind a dissociative shock. Hollenbach and McKee (1979) assumed a functional form for f_{gr} which has the efficiency falling to $\sim 10\%$ at a gas temperature of 1000 K (Burke and Hollenbach 1983). The surfaces of grains may be sufficiently rough that f_{gr} is near unity at all temperatures (Buch 1987). In view of the uncertainties we assumed unit efficiency in most of our shock models, but we investigated the case when f_{gr} is that adopted by Hollenbach and McKee (1979) and the case when it is zero and grain formation of H_2 does not occur.

Figures 3, 4, 5, and 6 of the abundance profiles of the components in the shocked gas refer to our standard models in which H_2 is formed with unit efficiency. For the standard models we adopted element abundances depleted only slightly below the solar values (Table 2) and a magnetic field strength of $B = n_0^{1/2}\ \mu$G. The figures all refer to a shock propagating into a preshock gas of 10^5 cm^{-3} with a velocity of 80 km s^{-1}.

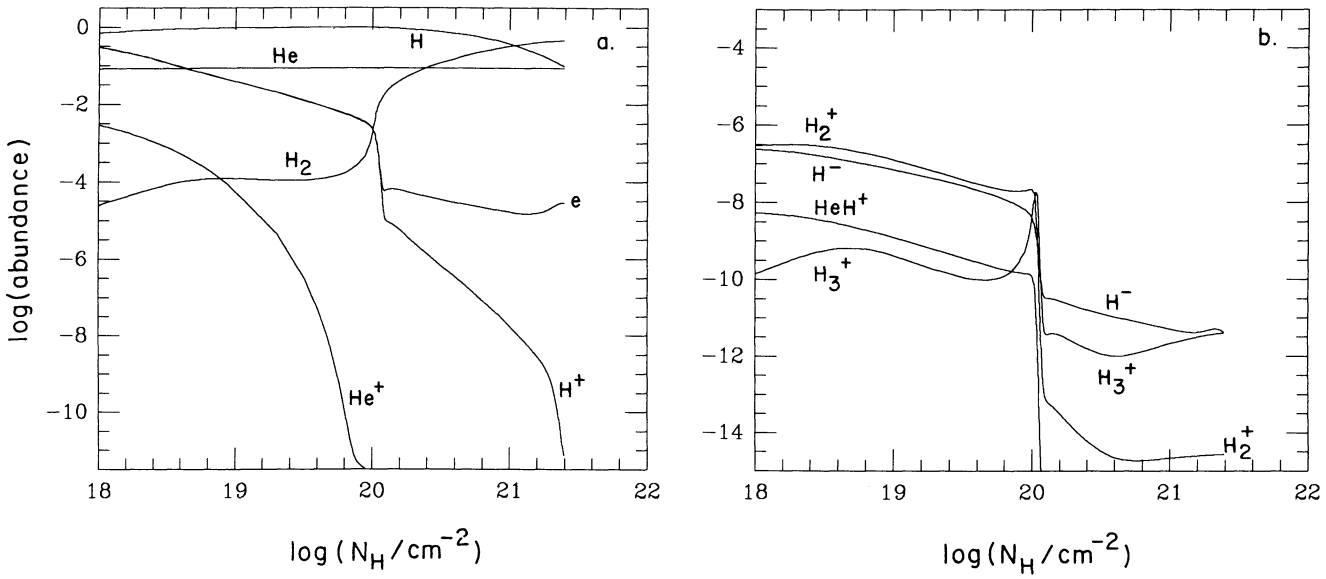

FIG. 3.—Abundance profiles of species containing hydrogen and helium, for a shock velocity of 80 km s^{-1} and a preshock density of 10^5 cm^{-3}

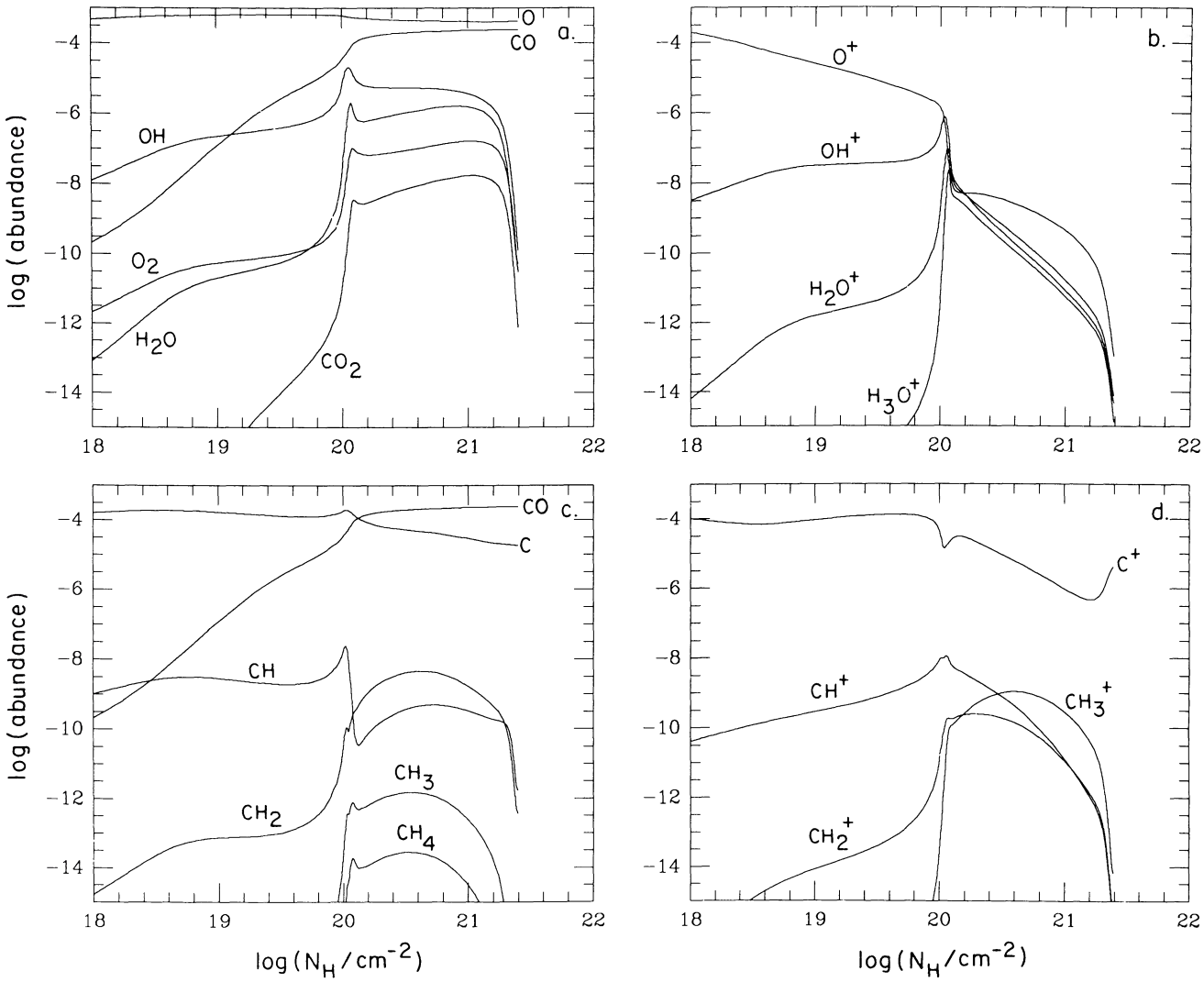

FIG. 4.—Abundance profiles of species containing oxygen and carbon, for a shock velocity of 80 km s^{-1} and a preshock density of 10^5 cm^{-3}

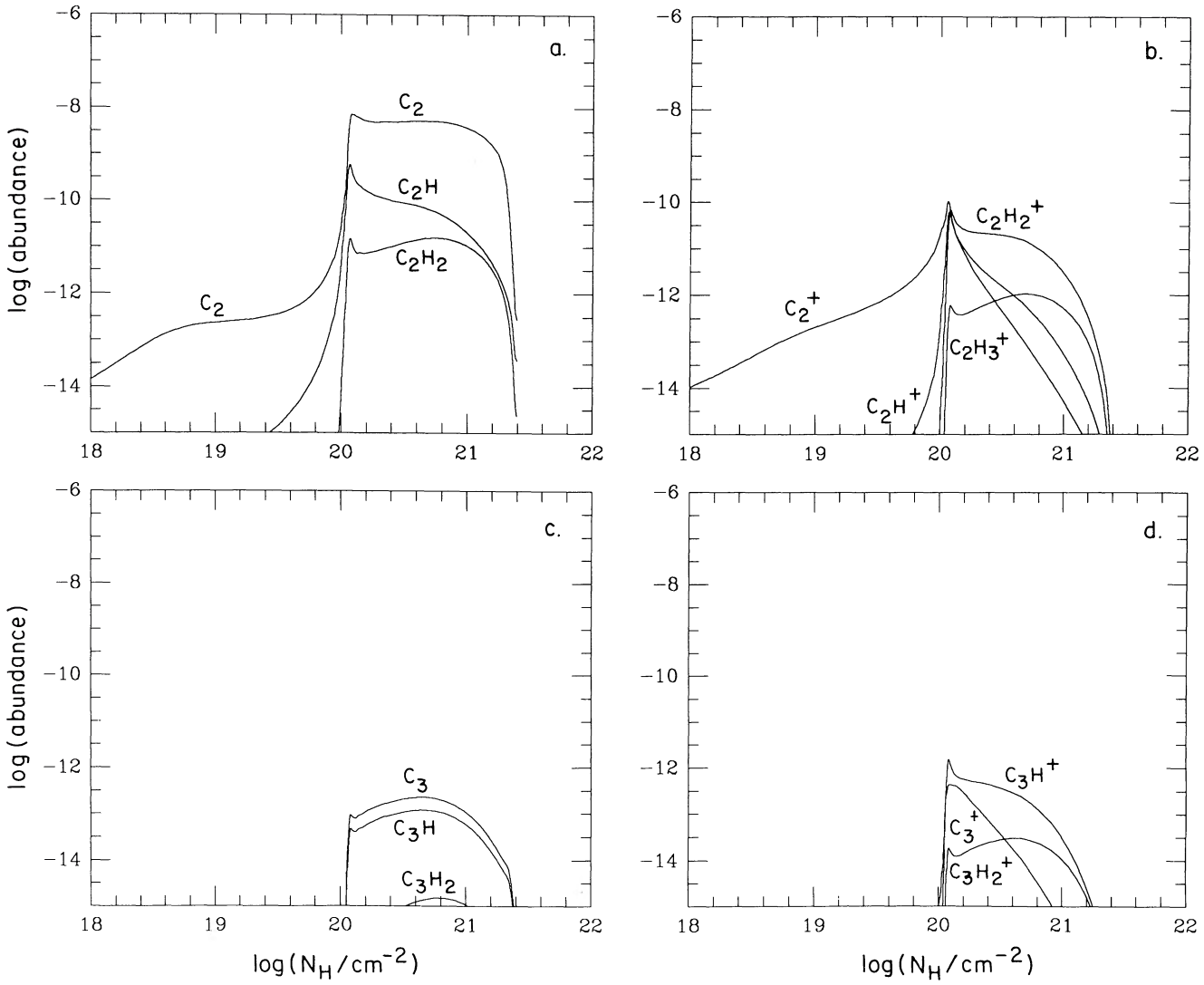

FIG. 5.—Abundance profiles of the complex hydrocarbons, for a shock velocity of 80 km s^{-1} and a preshock density of 10^5 cm^{-3}

At high temperature molecular hydrogen is destroyed by the endothermic reaction with H^+:

$$H_2 + H^+ \rightarrow H_2^+ + H ,$$

by collisional dissociation:

$$H_2 + H \rightarrow H + H + H ,$$

and by the charge transfer reaction:

$$H_2 + He^+ \rightarrow H + H^+ + He + 6.5 \text{ eV} ,$$

which is slow for H_2 in its lowest vibrational level, but fast for H_2 in the excited $v = 2$ state (Jones *et al.* 1986). We adopted as the effective rate coefficient the $v = 2$ value multiplied by the thermal population of the $v = 2$ state. We found the reaction to be a significant mode of destruction of H_2 at high temperature.

Photodissociation of H_2 takes place following line absorption in the Lyman and Werner bands. Self-shielding by the H_2 absorption lines ensures that even a precise coincidence of an absorption line with one of the strong lines emitted by the hottest part of the gas would not cause significant destruction of H_2.

Abundance profiles of H_2 are shown in Figure 3*a*. They demonstrate that the formation of H_2 does not reach completion until the gas temperature has fallen to a few hundred degrees.

b) Formation of HeH^+

The molecular ion HeH^+ is formed directly from its atomic constituents in the early phases of molecule reformation behind a fast shock. The formation and destruction mechanisms for HeH^+ have been discussed by Black (1978) and by Roberge and Dalgarno (1982).

In the cooling gas behind a dissociative shock that is fast enough ($v_0 \geq 100$ km s^{-1}) to ionize helium, two formation mechanisms are of comparable importance; they are radiative association of He^+ and H:

$$He^+ + H \rightarrow HeH^+ + h\nu ,$$

and Penning ionization of helium in the metastable $2\,^3S$ state:

$$He(2\,^3S) + H \rightarrow HeH^+ + e .$$

Because excited $He(2\,^3S)$ atoms are produced by radiative recombination to triplet states of helium and at densities above 3000 cm^{-3} are destroyed predominantly by electron-impact excitation to singlet states, the abundance of the metastable atoms bears a constant ratio to that of He^+. The total formation rate of HeH^+ may therefore be written:

$$r_{HeH^+} = n(He^+)n(H)\left(k_{ra} + \frac{\alpha_T}{q_S} k_{pi}\right), \tag{30}$$

where k_{ra} and k_{pi} are the rate coefficients for the radiative association and Penning ionization reactions, α_T is the total rate coefficient for radiative recombination to triplet states of helium, and q_S is the total rate coefficient for electron-impact excitation from $He(2\,^3S)$ to singlet states.

In the case of slower shocks that do not produce significant concentrations of He^+, the major means of formation of HeH^+ is by an endothermic proton transfer from H_2^+:

$$He + H_2^+ \rightarrow HeH^+ + H - 0.8 \text{ eV} .$$

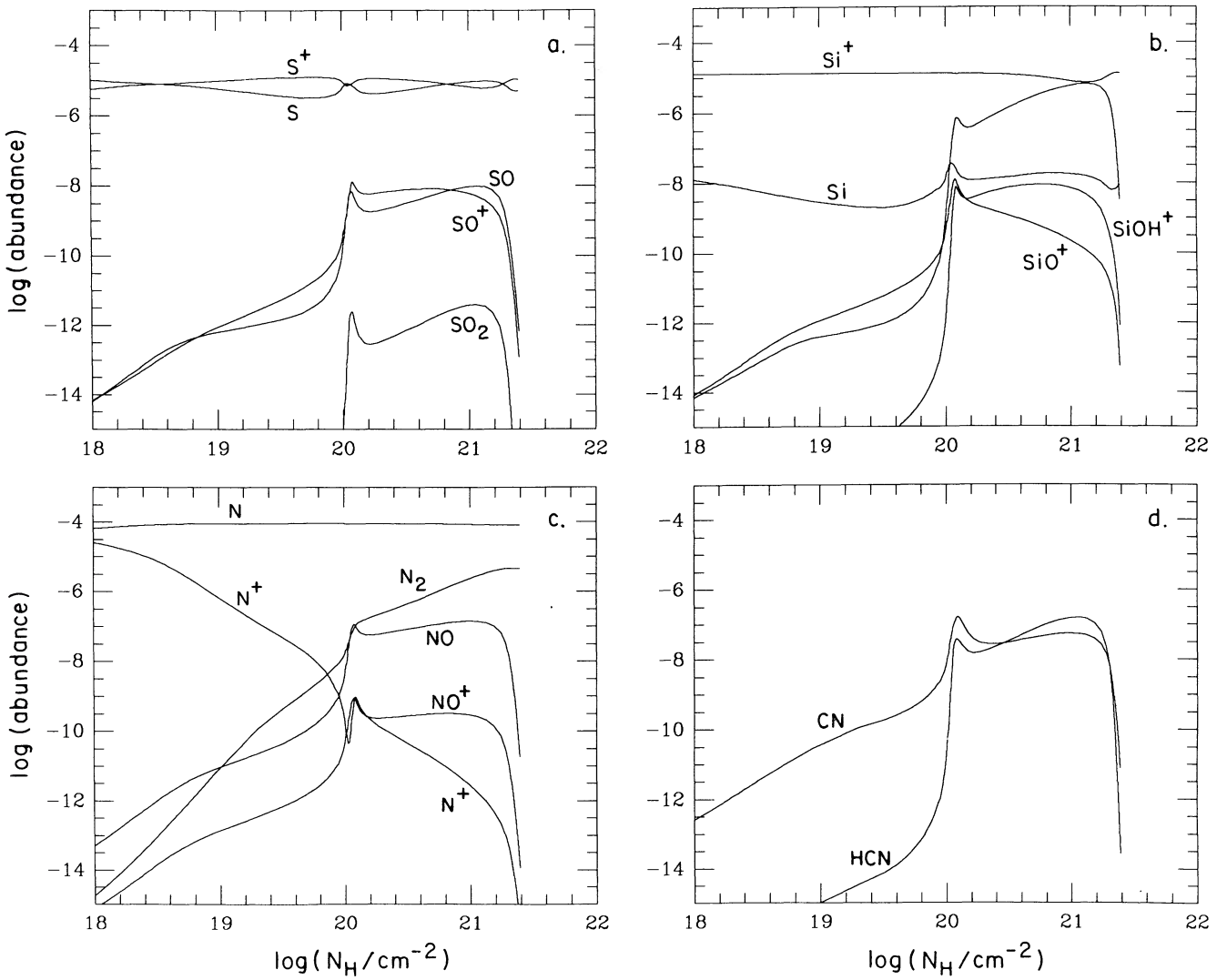

FIG. 6.—Abundance profile of species containing sulphur, silicon, and nitrogen, for a shock velocity of 80 km s^{-1} and a preshock density of 10^5 cm^{-3}

TABLE 2

ELEMENTAL ABUNDANCES

Element	Abundance
Hydrogen	1
Helium	8.5×10^{-2}
Carbon	2.6×10^{-4}
Nitrogen	9.1×10^{-5}
Oxygen	6.6×10^{-4}
Neon	1.0×10^{-4}
Magnesium	1.0×10^{-5}
Silicon	1.3×10^{-5}
Sulphur	1.6×10^{-5}
Argon	7.9×10^{-6}
Calcium	7.9×10^{-7}
Iron	1.6×10^{-5}

Photodissociation is unimportant at photon energies below the Lyman limit, and the main destruction path is proton transfer to H:

$$HeH^+ + H \rightarrow He + H_2^+ .$$

Substantial abundances of HeH^+ are achieved when the shock velocity is 90 km s^{-1} or greater, enough to ionize helium significantly, opening the possibility that vibrationally excited HeH^+ emission of detectable intensity might be produced in regions subject to a dissociative shock.

c) *Formation of* H_2^+ *and* H_3^+

The molecular ion H_2^+ is also produced in the early stages of molecule reformation. Production is by means of the proton transfer reaction that destroys HeH^+, given above, as well as by radiative association of H and H^+:

$$H + H^+ \rightarrow H_2^+ + h\nu .$$

At lower temperatures where the ionization fraction is small, cosmic-ray ionization of H_2 becomes the major formation mechanism. The ion is destroyed by charge transfer to H:

$$H_2^+ + H \rightarrow H_2 + H^+ ,$$

by dissociative recombination, and by proton transfer to H_2 with the production of H_3^+:

$$H_2^+ + H_2 \rightarrow H_3^+ + H .$$

We assume that the dissociative recombination of H_3^+ is slow (Smith and Adams 1984), so that H_3^+ is destroyed mostly by proton transfer to neutral species such as C, O, and CO.

Figure 7 summarizes the network of reactions involved in the formation of HeH^+, H_2^+, and H_3^+, and Figure 3*b* shows the abundance profiles for a shock velocity of 80 km s^{-1} and a preshock density of 10^5 cm^{-3}.

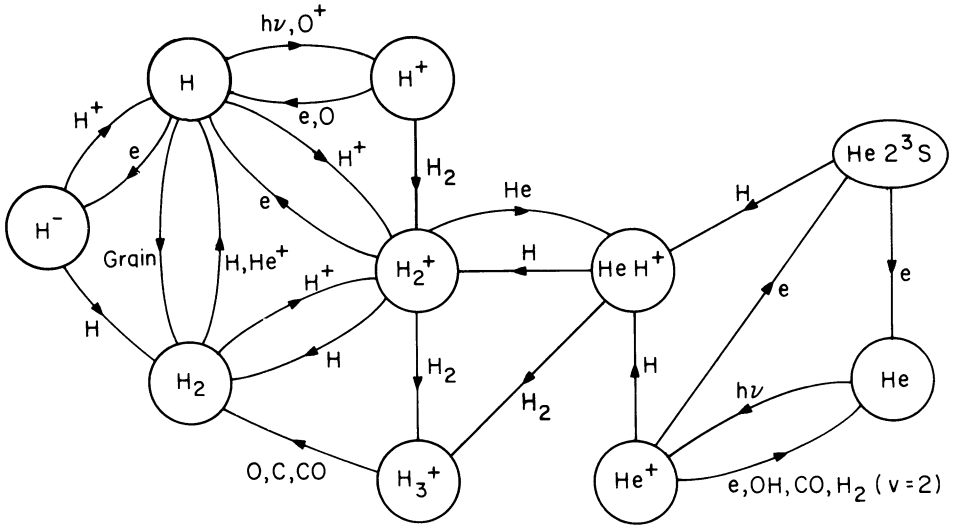

FIG. 7.—Chemistry of the hydrogen and helium species

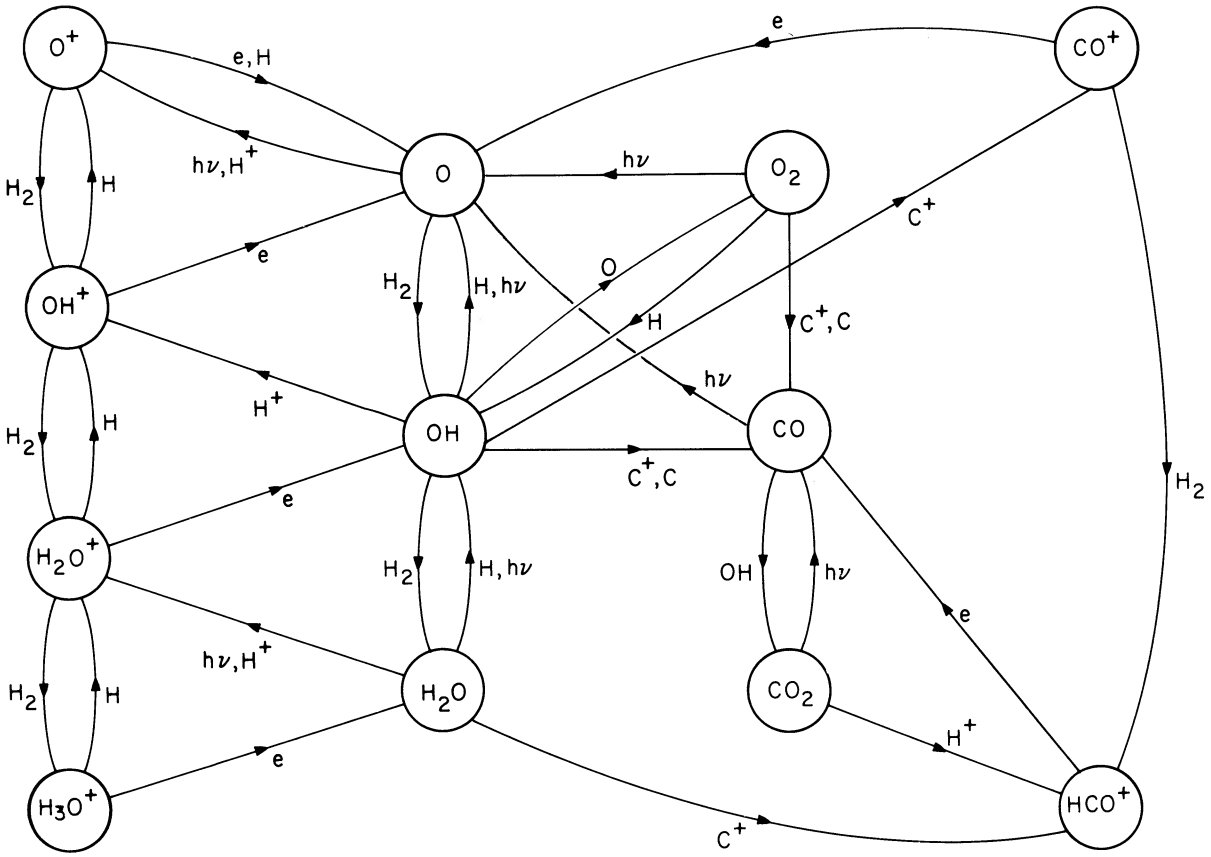

FIG. 8.—Chemistry of oxygen-bearing species

d) Chemistry of Oxygen Species and the Formation of Coolants

The formation of molecular hydrogen is followed by a series of reactions which produce molecules containing oxygen; such molecules include the important coolants OH, H_2O, and CO. Figure 8 summarizes the relevant chemical network. The abundance profiles calculated for the neutrals O, OH, H_2O, O_2, CO, and CO_2 are shown in Figure 4*a*, and those computed for the ions OH^+, H_2O^+, and H_3O^+ appear in Figure 4*b*.

The molecules OH and H_2O are formed by a sequence of hydrogen atom abstractions:

$$O + H_2 = OH + H$$

$$OH + H_2 = H_2O + H\ .$$

The first reaction is endothermic in the forward direction, and the second is exothermic but has a large activation energy barrier. We adopt the rate coefficients recommended by Wagner and Graff (1987) for vibrationally cold OH and H_2O but with the H_2 rotational levels thermally populated. The sequence is mediated by the reverse reactions with H and by the effects of photodissociation:

$$OH + h\nu \rightarrow O + H\ ,$$

$$H_2O + h\nu \rightarrow OH + H\ .$$

The photodissociation cross sections at the Lyα frequency are, respectively, 2×10^{-18} and 1.6×10^{-17} cm^2 (van Dishoeck and Dalgarno 1984; Kley 1984).

The abundance profiles show an OH concentration increasing slowly with the molecular hydrogen fraction, reaching a peak abundance of a few percent of the total oxygen abundance, and finally diminishing rapidly when the gas temperature falls below the level at which the endothermic production reaction is effective. The H_2O concentration remains below that of OH until a substantial molecular hydrogen fraction has been achieved and a sufficient column density built up behind the shock front that dust absorption significantly attenuates the destructive radiation field. This behavior is different from that predicted by models of nondissociative shocks in dense molecular clouds (Iglesias and Silk 1978; Chernoff, Hollenbach, and McKee 1982; Draine, Roberge, and Dalgarno 1983), where the absence of photodissociating radiation and the low abundance of atomic hydrogen permit almost all gas phase oxygen to be incorporated into H_2O, which consequently becomes the most abundant molecule after H_2 and the major coolant in nondissociative shocks.

The molecular ions OH^+, H_2O^+, and H_3O^+ are produced in a series of hydrogen abstractions analogous to those which give rise to OH and H_2O:

$$O^+ + H_2 = OH^+ + H ,$$
$$OH^+ + H_2 = H_2O^+ + H ,$$
$$H_2O^+ + H_2 = H_3O^+ + H .$$

All these reactions are exothermic in the forward direction and possess negligible activation energy barriers. The sequence is mediated by dissociative recombination of OH^+, H_2O^+, and H_3O^+, producing O, OH, and H_2O. Dissociative recombination is not a significant source of OH and H_2O, however, and the main importance of the ion-neutral reactions given above is in facilitating the recombination of O^+: reaction of O^+ with H_2 followed by dissociative recombination to O is a more effective recombination route than direct radiative recombination of O^+ with electrons. The state of ionization of oxygen is of particular importance because once the fractional ionization falls below about 3×10^{-3} it controls the ionization equilibrium of hydrogen via the near-resonant charge exchange:

$$O + H^+ = O^+ + H .$$

Carbon monoxide is formed predominantly by reaction of C^+ with OH:

$$C^+ + OH \rightarrow CO + H^+$$
$$\rightarrow CO^+ + H .$$

The CO^+ produced in the second reaction path may also contribute to CO formation, either by undergoing charge exchange with H or via the sequence

$$CO^+ + H_2 \rightarrow HCO^+ + H ,$$
$$HCO^+ + e \rightarrow CO + H .$$

Because CO is the most strongly bound diatomic molecule, it is not easily destroyed. The only significant destruction modes are photodissociation and dissociative charge transfer to He^+:

$$CO + He^+ \rightarrow C^+ + O + He .$$

Destruction by dissociative charge transfer is diminished in hot gas because He^+ is removed by reactions with H_2.

Photodissociation of CO is initially effective in preventing the complete conversion of carbon to CO, as the abundance profiles in Figure 4*c* illustrate. Unlike H_2 self-shielding, CO self-shielding does not immediately come into play because carbon has a far smaller elemental abundance than hydrogen. Eventually, however, a sufficient CO column density is built up that self-shielding moderates the photodissociation rate.

Molecular oxygen and carbon dioxide are produced in the reactions:

$$O + OH \rightarrow O_2 + H ,$$
$$CO + OH \rightarrow CO_2 + H .$$

O_2 and CO_2 are destroyed primarily by photodissociation and photoionization.

e) Carbon Chemistry and the Formation of Complex Species

Our reaction network for the carbon chemistry is similar to that adopted by Pineau des Forets *et al.* (1987) and summarized schematically in their Figure 1. Both neutral and singly ionized hydrocarbon species undergo hydrogen atom abstraction reactions analogous to those discussed above for the oxygen hydrides:

$$C_nH_m + H_2 = C_nH_{m+1} + H ,$$
$$C_nH_m^+ + H_2 = C_nH_{m+1}^+ + H ,$$

although in contrast to the oxygen analog, the initiating reaction

$$C^+ + H_2 \rightarrow CH^+ + H$$

is endothermic. For the neutral-neutral sequence involving two-carbon molecules, the activation energies are not known, and for the three-carbon neutrals even the heats of formation, and therefore the heats of reaction, are not known. We therefore exclude such reactions from the network with the exception of

$$C_2H + H_2 \rightarrow C_2H_2 + H ,$$

for which Mitchell (1984) assumed an activation energy of 1450 K.

Carbon-carbon bonds are created in ion-neutral reactions such as

$$C^+ + C_nH_m \rightarrow C_{n+1}H_{m-1}^+ + H ,$$
$$C + C_nH_m^+ \rightarrow C_{n+1}H_{m-1}^+ + H .$$

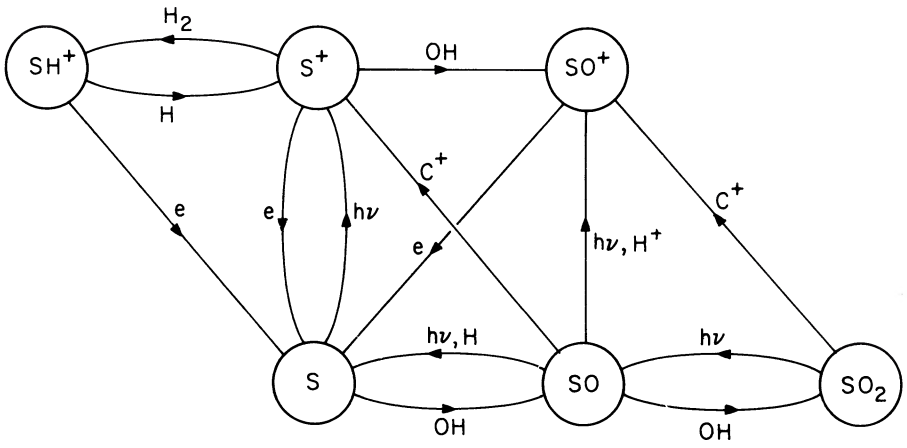

FIG. 9.—Chemistry of the sulphur-bearing species

In addition to being produced in such reactions, C_2 is also formed by a sequence initiated by reaction of HCN with C^+:

$$HCN + C^+ \rightarrow C_2N^+ + H ,$$

$$C_2N^+ + e \rightarrow C_2 + N .$$

Formation of a C-C bond is invariably accompanied by destruction of a C-H bond, so concatenation of carbon atoms can only take place after the molecular hydrogen fraction has become large enough to replenish the total number of C-H bonds by hydrogen abstraction reactions.

Hydrocarbons are destroyed in reactions with atomic oxygen and by photodissociation and photoionization. Except in the case of CH, CH_4, C_2, and C_2H_2, none of the photodestruction cross sections is known. We use a generic estimate of 10^{-17} cm^2 for the photodestruction cross section, and at photon energies above the ionization potential we assume a photoionization yield of 50%. We assume all the neutral hydrocarbons react with atomic oxygen except for C_3H and C_3H_2. The abundance profiles are shown in Figure 5 for a shock velocity of 80 km s^{-1} and a density of 10^5 cm^{-3}. The results must be regarded as qualitative because of uncertainties in the hydrocarbon chemistry.

f) *Sulphur, Nitrogen, and Silicon Chemistry*

Figures 9, 10, and 11 show the chemical networks involving species containing sulphur, nitrogen, and silicon. The abundance profiles of the S, N, and Si species are presented in Figure 6.

The OH molecule proves to be crucial in the chemistry of all three elements. The neutral hydrides SH and H_2S are less strongly bound than their oxygen analogs, with the result that both the reactions

$$S + H_2 = SH + H ,$$

$$SH + H_2 = H_2S + H ,$$

are endothermic. The activation energy for the first reaction is considerably greater than in the corresponding oxygen reaction, and significant abundances of SH and H_2S are never achieved. By the time a sufficient molecular hydrogen fraction has been established, the gas is too cool to permit hydrogen atom abstraction.

The major sulphur-bearing species is SO, formed in the reaction:

$$S + OH \rightarrow SO + H ,$$

and destroyed by photodissociation and by charge exchange with H^+:

$$SO + H^+ \rightarrow SO^+ + H .$$

The molecular ion SO^+ is produced by the charge exchange reaction, and directly from OH:

$$S^+ + OH \rightarrow SO^+ + H .$$

Destruction of SO^+ takes place by means of dissociative recombination. Sulphur monoxide is slowly converted to sulphur dioxide in a reaction with OH:

$$SO + OH \rightarrow SO_2 + H .$$

Sulphur dioxide is destroyed by photodissociation.

Because the ionization threshold for atomic nitrogen lies shortward of the Lyman limit, N^+ is no longer replenished by photoionization of N once the optical depth in atomic hydrogen becomes large. N^+ is therefore rather rapidly destroyed by

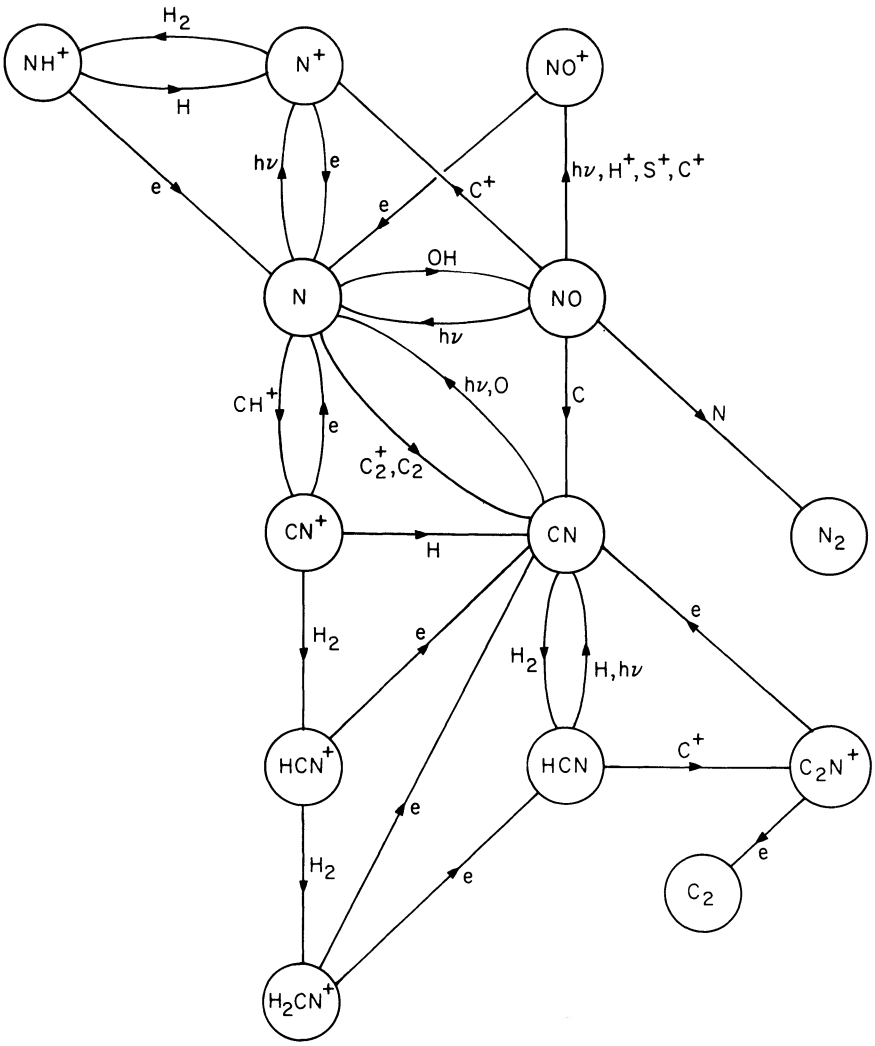

FIG. 10.—Chemistry of the nitrogen-bearing species

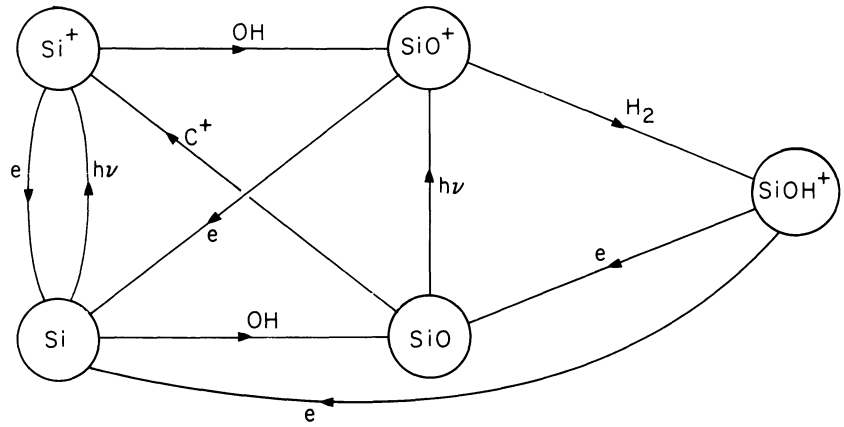

FIG. 11.—Chemistry of the silicon-bearing species

radiative recombination and by the sequence:

$$N^+ + H_2 \rightarrow NH^+ + H ,$$
$$NH^+ + e \rightarrow N + H .$$

The first reaction is slightly endothermic.

Hydrogen abstraction from H_2 by atomic nitrogen is considerably endothermic, just as in the case of atomic sulphur, and once again it is reaction with OH that dominates the nitrogen chemistry:

$$N + OH \rightarrow NO + H .$$

Nitric oxide is destroyed by photodissociation and photoionization, and undergoes reactions with atomic carbon, to produce cyanogen:

$$NO + C \rightarrow CN + O ,$$

and with atomic nitrogen, to produce molecular nitrogen:

$$NO + N \rightarrow N_2 + O .$$

Cyanogen is also formed in the reaction

$$C_2 + N \rightarrow CN + C .$$

It is destroyed by atomic oxygen,

$$CN + O \rightarrow CO + N ,$$

and may abstract a hydrogen atom from H_2 to form HCN,

$$CN + H_2 = HCN + H ,$$

a reaction which is exothermic in the forward direction. For shock velocities above 80 km s^{-1}, photodissociation by photons of energy above 12 eV is an additional means of destruction of CN.

Cyanogen and hydrogen cyanide are also produced by dissociative recombination of HCN^+ and H_2CN^+, molecular ions which are formed by the sequence:

$$N + CH^+ \rightarrow CN^+ + H ,$$
$$CN^+ + H_2 \rightarrow HCN^+ + H ,$$
$$HCN^+ + H_2 \rightarrow H_2CN^+ + H .$$

Hydrogen cyanide is photodissociated by Lyα radiation and, in faster shocks, by C III 97.7 nm photons. It is destroyed by reaction with C^+:

$$HCN + C^+ \rightarrow C_2N^+ + H .$$

Molecular nitrogen is a strongly bound molecule which undergoes chemical reactions only with He^+ and H_3^+, ions which are trace species in the region where N_2 is formed. Photodissociation of N_2 is apparently only possible at wavelengths shortward of 100 nm, by absorptions into predissociated excited states (van Dishoeck 1987). The oscillator strengths and natural line widths of the absorbing transitions are uncertain. N_2 photodissociation is probably of negligible importance in fast shocks, and, once converted to N_2, nitrogen remains in that form throughout the time period covered in our calculations. The OH abundance falls off before conversion to N_2 is complete, however, and the formation of NO and N_2 is interrupted. In its most abundant isotopic form, N_2 has no dipole moment and is undetectable at far-infrared or radio wavelengths, although the protonated species, N_2H^+, has been identified in dense interstellar clouds (Green, Montgomery, and Thaddeus 1974). The isotopically substituted $^{14}N^{15}N$ molecule does possess a small dipole moment that, in principle, permits its detection at radio frequencies.

Neither Si nor Si^+ reacts rapidly with molecular hydrogen, the abstraction reactions leading to SiH and SiH^+ each having an endothermicity in excess of 10^4 K. It is the reaction with OH that initiates the formation of silicon molecular species:

$$Si + OH \rightarrow SiO + H ,$$
$$Si^+ + OH \rightarrow SiO^+ + H .$$

Unlike the analogous reaction of C^+, the reaction

$$Si^+ + OH \rightarrow SiO + H^+$$

is endothermic and is not a significant reaction channel.

The molecular ion SiO^+ is presumed to undergo rapid dissociative recombination, but may also react exothermically with molecular hydrogen to produce $SiOH^+$:

$$SiO^+ + H_2 = SiOH^+ + H .$$

The reverse reaction is too endothermic to be a significant means of destruction of $SiOH^+$, and $SiOH^+$ is most likely to undergo dissociative recombination. Quantal calculations by Wilson (1978) have shown the structure of $SiOH^+$ to be Si–O–H^+ (in contrast to that of the carbon analog, O–C–H^+.) We assume that one-third of dissociative recombinations lead to H + SiO and two-thirds to Si + OH.

Silicon monoxide is destroyed by C^+, forming the more strongly bound carbon monoxide molecule,

$$SiO + C^+ \rightarrow CO + Si^+ ,$$

and by photoionization above its ionization potential of 11.64 eV.

Because the strength of the radiation field crucially affects how rapidly SiO is destroyed, the extent of conversion of silicon into SiO depends sensitively on the shock velocity. This velocity dependence is discussed further in § V below.

V. RESULTS AND DISCUSSION

a) The Temperature Structure

The rates of heating and cooling and the temperature structure for our standard model with a shock velocity of 80 km s^{-1} and a preshock density of 10^5 cm^{-3} are shown in Figures 12 and 13. At the initial temperature of 10^4 K, photoionization heating keeps the gas warm until a sufficient column density of atomic hydrogen is built up to shield the gas from radiation shortward of the Lyman limit. A further heat source results from the collisional de-excitation of trace amounts of H_2 that are pumped by Lyα radiation. The gas cools slowly until at $\sim$4000 K enough H_2 forms to create an OH abundance of 10^{-6}. Rotational excitation of OH becomes the major cooling process, and the cooling rate rises with decreasing temperature following the increasing OH abundance. A rapid drop in temperature ensues to below 1000 K at which point the OH abundance and the OH cooling decrease because of the declining effectiveness of the endothermic production route to OH.

The sharp drop in temperature is followed by a second plateau where the cooling, dominated still by rotational transitions of OH, is balanced by the heating that results from H_2 formation on grains. CO rotational transitions and [O I] fine-structure emission contribute significantly to the cooling in this plateau region, and once the temperature falls below 500 K, neutral oxygen becomes the major coolant. Eventually, at $\sim$400 K, H_2 formation is largely complete, and the heating associated with this process starts to decrease. The temperature undergoes a second period of rapid decline and falls below 200 K, at which point our calculation is terminated.

With a preshock density of 10^6 cm^{-3}, the temperature profile, shown in Figure 14, is qualitatively similar to that computed for the $n_0 = 10^5$ cm^{-3} case. However, the cooling rate per atom during the initial phase does not increase in proportion to the preshock density because many of the atomic transitions which dominate the cooling are quenched by collisional de-excitation. The Lyα heating rate per absorbing H_2 molecule does increase linearly with the preshock density, with the result that the sudden temperature drop between 4000 and 1000 K is delayed. In the second plateau region, collisional de-excitation reduces the effectiveness of CO and [O I] cooling, resulting in a larger total column density out to the point at which the temperature drops below 200 K.

In the case where the preshock density is 10^4 cm^{-3} similar considerations apply in the opposite sense, resulting in the temperature profile shown in Figure 15. In this lower density case, atoms become the major coolants throughout the shocked gas region. As the preshock density falls from 10^5 to 10^4 cm^{-3}, the cooling resulting from [O I] fine-structure emission decreases only in proportion to n_0, due to the effects of collisional de-excitation. The rate of chemical reactions and the heating associated with H_2 formation are both proportional to n_0^2, and reformation of molecular hydrogen is therefore only partially complete by the time the gas has cooled

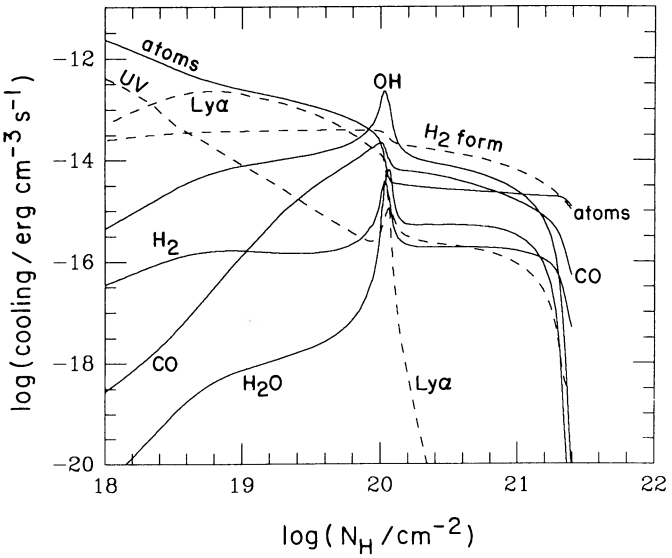

FIG. 12.—Rates of heating and cooling processes per unit volume, for a shock velocity of 80 km s^{-1} and a preshock density of 10^5 cm^{-3}. *Solid lines*, cooling processes; *dashed lines*, heating processes.

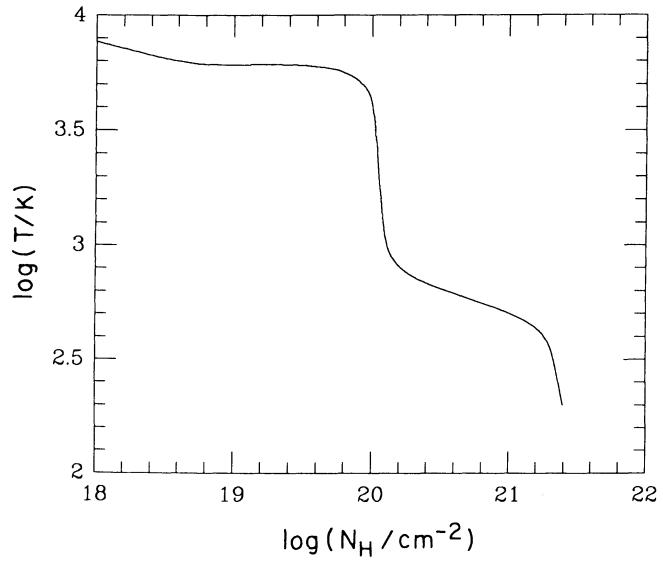

FIG. 13.—Temperature profile, for a shock velocity of 80 km s^{-1} and a preshock density of 10^5 cm^{-3}.

to 200 K. If the presence of an energy barrier causes the collisional de-excitation rate to drop rapidly when $T \leq 200$ K, the remaining chemical energy is released in quadrupole rovibrational transitions of H_2; otherwise the energy release results in a second temperature plateau in gas cooler than 200 K.

b) Chemical Composition

The column densities of atomic, ionic, and molecular constituents obtained in the cooling gas behind a dissociative shock are given in Table 3 for shock velocities of 60, 80, 90, and 100 km s^{-1} and preshock densities of 10^4, 10^5, and 10^6 cm^{-3}. The column densities of many of the simple molecules may exceed 10^{14} cm^{-2}, but those of the complex hydrocarbons are always less than 10^{13} cm^{-2}. Except for HeH^+, the column densities of the molecular ions listed may exceed 10^{12} cm^{-3}. The composition is markedly different from that which occurs in the cooling gas behind a slower nondissociative shock because the chemistry takes place in a destructive radiation field, the ionization fraction is much greater and the molecular hydrogen fraction is small in the warm region of the shocked gas, becoming large only where the gas has cooled.

The composition of the neutral and ionized molecules is greatly affected by the role of OH as an intermediary leading to the formation of oxides rather than hydrides. Thus NO is more abundant in the postshock gas than NH, SiO more abundant than SiH, and SO^+ more abundant than SH^+.

Photodissociation tends to limit the abundances of the molecular species, although photodissociation of larger molecules augments the abundances of the diatomic systems and photodissociation of CO is a source of neutral carbon atoms for the

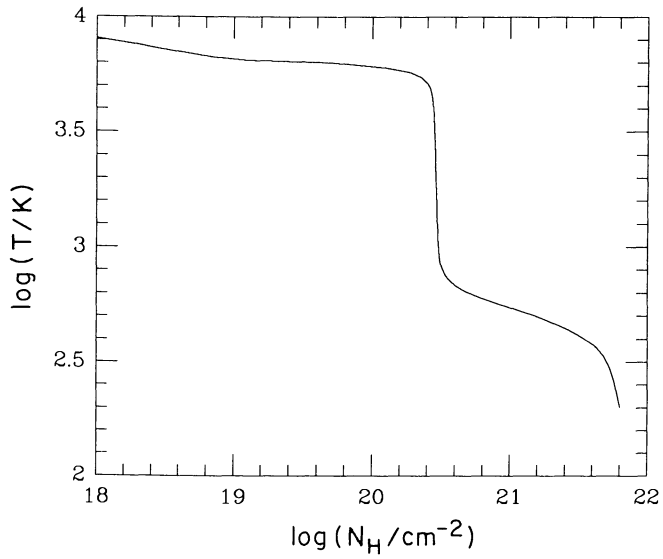

FIG. 14.—Temperature profile, for a shock velocity of 60 km s^{-1} and a preshock density of 10^6 cm^{-3}.

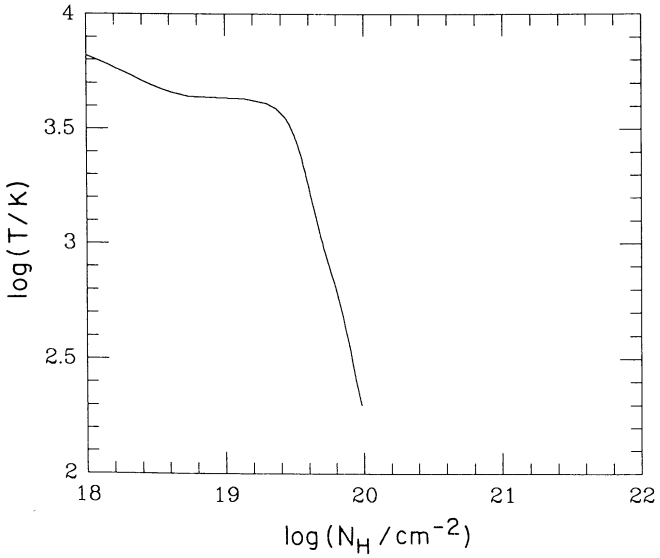

FIG. 15.—Temperature profile, for a shock velocity of 60 km s^{-1} and a preshock density of 10^4 cm^{-3}.

formation of hydrocarbons. The effect of the additional C atoms on the complex hydrocarbons is countered by photodissociation and photoionization, by the small fraction of warm molecular hydrogen, and by the efficient conversion of carbon into CO resulting from the high fraction of carbon in the form of C^+. The resulting abundances of complex hydrocarbons are small.

When the preshock density is 10^5 cm^{-3} or greater, column densities of many of the diatomic molecules show a decrease with increasing shock velocity because faster shocks produce more photodestructive radiation. This trend is particularly marked in molecules such as SiO and CN which are photodissociated or photoionized only by radiation shortward of the Lyα line, because the flux of such radiation is enhanced by a large factor as the shock velocity increases from 80 km s^{-1} to 100 km s^{-1}(see Table 1). The column densities produced of SO and HCN show a similarly strong decline with increasing shock velocity because the species from which they are formed, S and CN, are themselves only destroyed by radiation shortward of 121.6 nm. The effect is enhanced in SiO because C^+ ions, which also destroy the molecule, are produced by photoionization of C by photons of energy above 11.3 eV.

The column densities of the neutral molecules OH, H_2O, CO, SiO, NO, CN, HCN, N_2, and O_2 all increase with the preshock density, because they are produced by reaction sequences which involve OH as one of the intermediates, and are consequently only slowly produced once the temperature falls to 400 K and the OH production rate drops rapidly. At a preshock density of 10^4 cm^{-3}, only CO and OH attain column densities in excess of 10^{14} cm^{-2}, because the shocked gas cools so rapidly relative to the chemical time scale for grain surface formation that the molecular hydrogen fraction is still only a few percent at the point at which the gas cools below 400 K. At a preshock density of 10^5 cm^{-3}, the molecular hydrogen fraction is already greater than one-half by the time the temperature reaches 400 K, and the column densities of all the species listed above exceed 10^{14} cm^{-3}, at least for a shock velocity of 60 km s^{-1}. When the preshock density is raised to 10^6 cm^{-3}, a further modest increase in the column densities of neutral molecules results.

The ionization in the shocked gas accelerates the formation of molecular ions and the presence of substantial concentrations of diatomic molecular ions provides a potentially unique diagnostic probe of a dissociative shock propagating in a molecular gas. Many of the molecular ion column densities exceed 10^{12} cm^{-2}. The ions are produced in the warm region of the gas where electron impact excitation of vibrational levels is a highly efficient mechanism (Neufeld and Dalgarno 1989) leading to emission in the 3–4 μm infrared region. Of particular utility may be the ions OH^+ and SO^+ and in fast shocks HeH^+. Emission from vibrational levels of HCO^+ is not significantly excited in fast shocks because HCO^+ is only abundant in gas of temperature $\sim$600 K. Pure rotational transitions may be excited, although emission in the $J = 1 \rightarrow 0$ radio line is likely to be masked by contributions from cold regions.

The column density of CH^+ reaches a value of 1.2×10^{13} cm^{-2} for shocks with velocities above 80 km s^{-1} and preshock densities above 10^5 cm^{-3}. In our calculation we adopted the standard laboratory rate coefficient for dissociative recombination

$$CH^+ + e \rightarrow C + H$$

(Mul *et al.* 1981). There remains the possibility that the process is slow for CH^+ in its lowest energy level. The predicted column densities are increased by factors of $\sim$5 if dissociative recombination is omitted from the chemistry.

The atomic and ionic systems C, C^+, O, S, and Si^+ have observable transitions. The neutral carbon column density decreases with increasing shock velocity, while that of C^+ shows a corresponding increase, reflecting the change in the flux of radiation capable of photoionizing atomic carbon.

Neutral oxygen shows only a rather weak dependence of its column density on the shock velocity. There is no large variation in column density because in all the models neutral atomic oxygen becomes the major oxygen species once the shocked gas has recombined. Neutral sulphur, by contrast, is photoionized by radiation longward of the Lyman limit. The column density of S^+ therefore increases with the shock velocity while that of S decreases. Under none of the conditions we consider do molecules containing sulphur account for a major fraction of the elemental abundance.

The Si^+ column density is of special interest because observations of the 35 μm line of Si II from the shocked region in Orion-KL have been claimed as evidence for the presence of a dissociative shock (Haas, Hollenbach, and Erickson 1986). Although the ionization equilibrium between Si and Si^+ favors Si^+ throughout the shocked gas region in all of our models, for preshock densities of 10^5 cm^{-3} or greater and shock velocities of 80 km s^{-1} or less, Si^+ is largely converted to SiO by the reaction sequence:

$$Si^+ + OH \rightarrow SiO^+ + H ,$$
$$SiO^+ + H_2 \rightarrow SiOH^+ + H ,$$
$$SiOH^+ + e \rightarrow SiO + H .$$

Destruction of the SiO molecule by the radiation field is analogous to the case with CO, except that the ionization potential lies below the Lyman limit. Except when the grain optical depth becomes large and destruction by C^+ becomes important, the dominant destruction process is photoionization:

$$SiO + h\nu \rightarrow SiO^+ + e .$$

Photodissociation by Lyα radiation is energetically possible, but would only be important in the unlikely event of a coincidence with an absorption line leading to a predissociated excited state. With photoionization as the destruction process, and allowing for dissociative recombination of the SiO^+ intermediate in the formation sequence, we may write the ratio of the SiO and Si^+

TABLE 3

COLUMN DENSITIES (cm^{-2}) OF SELECTED SPECIES IN GAS WARMER THAN 200 K: STANDARD MODELS

n_0/cm^{-3}:	10^4	10^4	10^4	10^4	10^5	10^5	10^5	10^5	10^6	10^6	10^6	10^6
v_0/kms^{-1}:	60	80	90	100	60	80	90	100	60	80	90	100
O	6.0(16)	8.3(16)	1.1(17)	1.2(17)	1.0(18)	1.1(18)	1.1(18)	1.2(18)	2.5(18)	2.6(18)	2.6(18)	2.8(18)
C	1.9(16)	1.7(16)	1.9(15)	7.6(14)	1.3(17)	9.1(16)	2.2(16)	7.4(15)	1.4(17)			
C^+	3.9(15)	1.4(16)	4.0(16)	4.5(16)	5.3(15)	1.9(16)	2.0(17)	2.2(17)	1.4(16)			
Si^+	1.3(15)	1.8(15)	2.2(15)	2.4(15)	1.2(16)	2.4(16)	3.0(16)	3.2(16)	5.4(15)	7.5(15)	6.1(16)	7.9(16)
S	7.6(14)	4.7(14)	2.5(13)	9.3(12)	2.8(16)	1.9(16)	4.7(14)	1.6(14)	9.5(16)	9.6(16)	1.7(16)	6.8(15)
S^+	7.6(14)	1.7(15)	2.6(15)	2.9(15)	7.9(15)	2.1(16)	3.6(16)	3.9(16)	3.6(15)	1.1(16)	8.7(16)	1.0(17)
H_2	1.5(18)	2.3(18)	3.5(18)	4.6(18)	6.8(20)	7.6(20)	6.9(20)	7.4(20)	2.5(21)	2.8(21)	2.7(21)	2.9(21)
OH	3.4(14)	3.6(14)	3.6(14)	3.7(14)	5.7(15)	6.8(15)	6.6(15)	7.6(15)	2.7(16)	3.2(16)	3.7(16)	4.6(16)
H_2O	5.8(12)	6.4(12)	4.8(12)	4.5(12)	1.9(15)	2.0(15)	1.3(15)	1.1(15)	6.1(16)	6.3(16)	4.0(16)	3.6(16)
CO	2.3(15)	4.5(15)	2.1(15)	2.5(15)	4.6(17)	5.4(17)	3.9(17)	4.2(17)	1.5(18)	1.7(18)	1.6(18)	1.7(18)
SiO	3.7(12)	1.7(12)	1.3(11)	6.7(10)	1.8(16)	8.5(15)	1.7(14)	9.4(13)	7.8(16)	8.2(16)	2.3(16)	1.0(16)
SO	5.7(10)	2.6(10)	5.8(08)	1.9(08)	2.3(13)	1.2(13)	1.8(11)	6.2(10)	8.6(14)		1.8(14)	6.1(13)
NO	6.9(11)	6.3(11)	4.1(11)	3.1(11)	2.3(14)	2.0(14)	7.1(13)	5.1(13)	3.1(15)	2.3(15)	1.5(15)	1.3(15)
CN	2.5(12)	1.6(12)	8.9(10)	3.0(10)	1.9(14)	7.9(13)	6.7(12)	3.1(12)	8.2(14)		4.9(13)	1.1(13)
HCN	5.9(10)	5.4(10)	2.8(09)	7.9(08)	5.0(14)	1.7(14)	2.3(12)	6.0(11)	8.2(15)	5.9(15)	2.5(14)	2.7(13)
N_2	2.3(12)	3.3(12)	1.2(12)	9.0(11)	7.6(15)	6.9(15)	2.3(15)	1.7(15)	1.5(17)	1.4(17)	1.0(17)	9.2(16)
CO_2	4.1(09)	6.5(09)	1.7(09)	1.2(09)	2.9(13)	2.2(13)	1.1(12)	5.1(11)	1.2(15)		8.4(13)	3.6(13)
O_2	1.4(12)	9.1(11)	8.3(11)	8.1(11)	2.9(14)	2.3(14)	1.5(14)	1.6(14)	7.6(15)			
SO_2	4.4(06)	1.9(06)	3.0(04)	9.6(03)	9.8(09)	4.1(09)	3.3(07)	1.3(07)	4.6(12)		6.7(11)	2.4(11)
CH	6.3(11)	5.5(11)	8.0(10)	3.9(10)	8.8(11)	1.2(12)	2.8(13)	3.4(13)	1.3(12)			
CH_2	2.1(09)	5.1(09)	1.5(10)	1.6(10)	8.9(11)	3.5(12)	8.6(13)	1.0(14)	2.2(11)			
C_2	8.2(09)	1.8(10)	5.7(09)	3.4(09)	6.6(12)	6.2(12)	5.3(13)	5.9(13)	1.0(13)			
C_2H	1.4(09)	2.5(09)	7.5(08)	4.2(08)	4.5(10)	7.1(10)	4.7(12)	1.0(13)	3.8(10)			
C_2H_2	1.6(07)	2.5(07)	5.6(06)	3.1(06)	1.0(10)	1.6(10)	1.7(12)	3.3(12)	1.6(10)			
C_3	1.9(05)	2.0(05)	5.7(04)	5.2(04)	1.6(08)	2.0(08)	5.5(11)	1.3(12)	5.2(08)			
C_3H	9.3(04)	9.8(04)	2.9(04)	2.7(04)	8.5(07)	1.1(08)	3.1(11)	7.6(11)	3.0(08)			
C_3H_2	2.9(02)	3.0(02)	7.1(01)	7.2(01)	9.8(05)	1.5(06)	2.7(09)	6.8(09)	3.8(06)			
SH	1.0(11)	7.2(10)	3.2(09)	1.1(09)	1.7(11)	1.1(11)	5.1(09)	1.6(09)	3.3(11)		7.1(09)	3.3(09)
H_2S	1.3(07)	8.9(06)	4.3(05)	1.8(05)	2.2(07)	1.5(07)	8.6(05)	4.0(05)	3.2(07)		1.3(06)	7.2(05)
H_2CO	6.7(03)	1.3(04)	3.1(04)	2.0(04)	9.8(06)	3.3(07)	6.0(08)	4.2(08)	9.6(06)			
H_2^+	4.9(12)	6.1(12)	6.8(12)	5.3(12)	5.7(12)	5.7(12)	8.9(12)	5.3(12)	6.5(12)	9.2(12)	1.1(13)	1.2(13)
H_3^+	8.5(11)	4.2(11)	3.8(11)	3.2(11)	2.7(11)	1.8(11)	2.5(11)	1.7(11)	9.7(10)			
HeH^+	3.7(10)	5.4(10)	6.9(10)	8.3(10)	5.4(10)	6.0(10)	9.9(10)	9.0(10)	7.1(10)	9.7(10)	1.2(11)	1.5(11)
OH^+	1.9(13)	1.8(13)	1.7(13)	1.7(13)	1.8(13)	1.5(13)	2.1(13)	1.9(13)	1.5(13)	2.0(13)	2.7(13)	3.0(13)
CH^+	1.2(11)	3.8(11)	1.9(12)	2.0(12)	2.9(11)	9.7(11)	9.5(12)	1.0(13)	3.3(11)	8.7(11)	9.5(12)	1.2(13)
HCO^+	6.7(10)	1.3(11)	2.3(11)	2.5(11)	6.9(12)	1.4(13)	5.7(13)	5.9(13)	1.1(13)	4.1(13)	1.6(14)	1.5(14)
SO^+	3.8(10)	5.8(10)	4.7(10)	5.0(10)	5.6(12)	9.8(12)	4.4(12)	5.0(12)	1.8(13)			

concentrations in the unshielded region as:

$$\frac{n(\mathrm{SiO})}{n(\mathrm{Si}^+)} = \frac{k_1 f_{\mathrm{abs}} f_{\mathrm{SiO}}\, n(\mathrm{OH})}{\Gamma_{\mathrm{SiO}}(1 - f_{\mathrm{abs}} f_{\mathrm{SiO}})}, \tag{31}$$

where k_1 is the rate coefficient for the initial reaction of Si^+ with OH, Γ_{SiO} is the photodissociation rate per SiO molecule, f_{SiO} is the fraction of dissociative recombinations of $SiOH^+$ that lead to SiO + H, and f_{abs} is the fraction of SiO^+ ions undergoing hydrogen atom abstraction to form $SiOH^+$ rather than dissociative recombination, given by

$$f_{\mathrm{abs}} = \frac{k_2\, n(\mathrm{H_2})}{k_2\, n(\mathrm{H_2}) + k_3\, n(e)}, \tag{32}$$

where k_2 and k_3 are the rate coefficients for the two reactions:

$$\mathrm{SiO}^+ + \mathrm{H_2} \rightarrow \mathrm{SiOH}^+ + \mathrm{H}\,,$$

$$\mathrm{SiO}^+ + e \rightarrow \mathrm{Si} + \mathrm{O}\,.$$

The fraction f_{abs} is large when $n(H_2)/n(e)$ exceeds $10^4 T^{-1/2}$. The photodissociation rate may be estimated (following eq. [16]) as

$$\Gamma_{\mathrm{SiO}} \sim 3 \times 10^{-10} \left(\frac{v}{100\ \mathrm{km\ s^{-1}}}\right)^3 \left(\frac{n_0}{\mathrm{cm^{-3}}}\right) \left(\frac{\sigma}{10^{-17}\ \mathrm{cm^2}}\right) f_{\mathrm{rad}}\ \mathrm{s^{-1}}\,, \tag{33}$$

where σ is the SiO photoionization cross section and f_{rad} is the fraction of the shock energy that is radiated as photons of energy between the ionization potential of SiO and the Lyman limit. Substituting into equation (31), we obtain

$$\frac{n(\mathrm{SiO})}{n(\mathrm{Si}^+)} \sim 10^{-3} \left[\frac{n(\mathrm{OH})/n_{\mathrm{H}}}{3 \times 10^{-6}}\right] \left(\frac{x_m}{100}\right) \left(\frac{f_{\mathrm{abs}} f_{\mathrm{SiO}}}{1 - f_{\mathrm{abs}} f_{\mathrm{SiO}}}\right) \left(\frac{100\ \mathrm{km\ s^{-1}}}{v}\right)^3 \left(\frac{10^{-17}\ \mathrm{cm^2}}{\sigma}\right) \frac{1}{f_{\mathrm{rad}}}\,, \tag{34}$$

where $x_m \sim 10^2$ is the ratio of the density in the shocked molecular region to that in the preshock gas, and quantities other than f_{rad} and f_{SiO} have been expressed as ratios to the values that they typically attain.

The efficiency of SiO formation depends on the unknown branching ratio for the dissociative recombination to SiO + H. With our estimated value for f_{SiO} of $\frac{1}{3}$, equation (34) predicts that in a region that is unshielded by dust, and where the molecular hydrogen fraction is large enough that f_{abs} is near unity, the SiO concentration will exceed that of Si^+ when f_{rad} is less than $\sim 10^{-3}$. The values given by the shock model of Raymond (1979) for f_{rad} are 4×10^{-4}, 1.2×10^{-3}, 4×10^{-2}, and 9×10^{-2} for shock velocities, respectively, of 60, 80, 90, and 100 km s^{-1}. Equation (34) therefore suggests that provided $f_{abs} \sim 1$ conversion of Si^+ to SiO will be effective for shock velocities of 60 and possibly 80 km s^{-1}, resulting in a decrease in the Si^+ column density. The detailed shock calculations confirm this simple estimate, although when the preshock density is 10^4 cm^{-3}, the molecular hydrogen forms too slowly to allow a substantial fraction f_{abs} to be achieved before the gas cools below 400 K and the OH abundance drops. The effect of dust shielding, particularly in the models with the highest preshock density, increases slightly the maximum velocity at which production of SiO is effective.

Because the strengths of magnetic fields in dense clouds are not known with any certainty, we have carried out a calculation with an assumed preshock field of $0.1 n_0^{1/2}$ μG, 1/10 our standard value. The maximum compression attained by the shocked gas is therefore a factor of 10 greater. The molecular column densities obtained are less than in the standard case, as expected because the total cooling column in equation (9), N_{cool}, is an order of magnitude smaller. The lower preshock field shifts the molecular region to a position where the total column density is smaller and where dust shielding is less effective. However, the density in the molecular region is 10 times greater, while the unshielded radiation field is the same, so that relative to chemical reaction rates the destructive effects of the unshielded radiation field are a factor of 10 smaller.

These two effects on the efficiency of photodestruction approximately cancel in determining the C/C^+ column density ratio, which remains unchanged. For the complex hydrocarbons, which are not significantly shielded by dust even in the standard case, the increase in the rate of chemical formation rates relative to unshielded photodestruction rates can result in a dramatic increase in the molecular column densities, particularly for the three-carbon molecules, although with a shock velocity of 80 km s^{-1} and a preshock density of 10^5 cm^{-3} none of the column densities of the complex hydrocarbons exceeds 2×10^{11} cm^{-2}.

We have investigated the effect on the shock structure of assuming the gas phase carbon abundance to be greater than that of oxygen. Since shock velocities as large as 60 km s^{-1} evaporate the grain mantles onto which oxygen is likely to be depleted as water ice (Hollenbach and McKee 1979), the abundances assumed in this model apply to shocks which propagate in carbon-rich stellar ejecta.

As in the standard case, carbon monoxide is rapidly formed once a self-shielding column density is built up. After the formation is complete it is carbon rather than oxygen that is left over. The result is a substantial increase in the column densities of the carbon-bearing molecules, and a corresponding decrease in those of the oxygen species. Below 800 K, carbon monoxide is the major molecular coolant.

We have not investigated the effects of varying the assumed gas phase abundances of the other elements, although the abundances of nitrogen, silicon, and sulphur are in any case too small to affect the overall shock structure. We expect the abundance profiles of molecules containing these elements to scale simply with the elemental abundances.

We have also explored the effects of reducing the efficiency of grain formation of H_2. The main consequence is a delay in the formation of H_2 in the shocked gas. Because all molecules except HeH^+ and H_2^+ involve H_2 in their formation, production of them

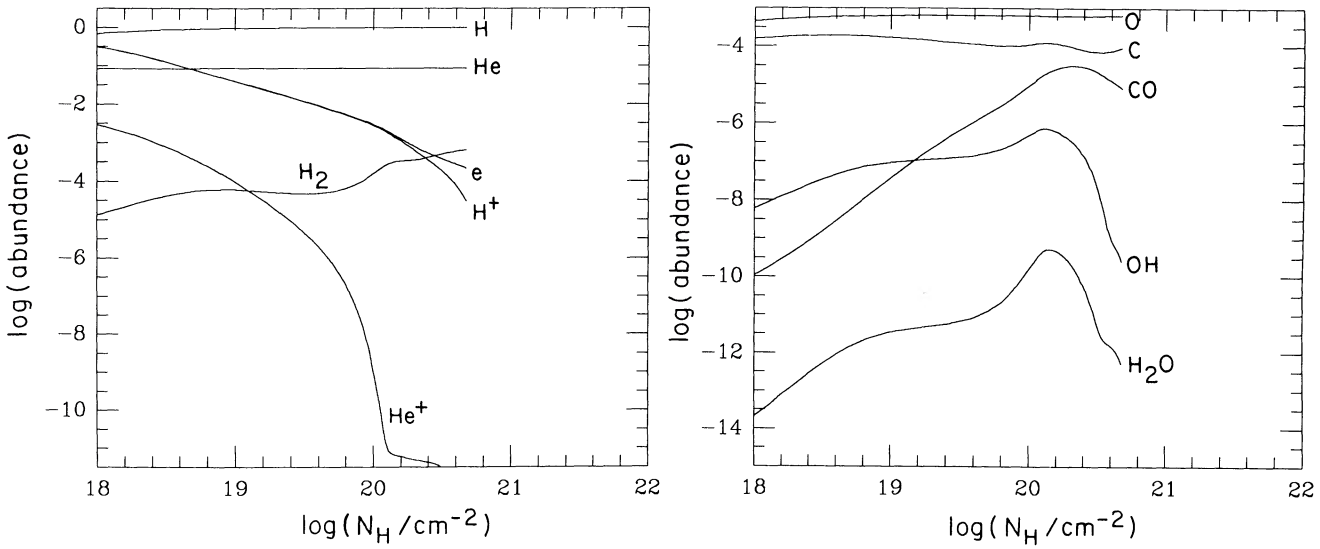

FIG. 16.—Abundance profiles without grain formation of H_2, for a shock velocity of 80 km s^{-1} and a preshock density of 10^5 cm^{-3}

is slowed down. The column densities of neutral species are substantially reduced, the temperature having fallen below the value required to overcome the activation energy barriers of crucial reactions before a significant H_2 fraction is achieved. Uncertainties in the physics of processes on grain surfaces clearly result in significant uncertainties in the structure of fast molecular shocks.

An associated effect of a lower H_2 formation efficiency is to extend to greater column densities the second plateau region in the temperature profile where the heating generated by H_2 production balances the cooling due to molecular transitions. Because the heating rate generated is now smaller, the plateau *temperature* is somewhat less. By the time the temperature has fallen to 200 K, H_2 formation is only 60% complete.

Figure 16 shows the abundance profiles that are obtained without H_2 formation on grain surfaces for a shock velocity of 80 km s^{-1} and a preshock density of 10^5 cm^{-3}. Molecular hydrogen forms via the H^- intermediate until the supply of electrons runs out as a result of radiative recombination; a maximum molecular fraction of 7×10^{-4} is achieved. The incorporation of carbon and oxygen into CO via the OH intermediate is moderately efficient despite the small molecular fraction. In our model, carbon monoxide reaches a peak abundance of 2×10^{-5}, falling eventually to 3×10^{-6}. The shocked gas has a final H_2/CO abundance ratio of 250, an unusually small value. These results have indirect application to pregalactic shocks prior to grain formation (Ostriker and Cowie 1981). With a preshock density of 10^5, atomic cooling dominates the thermal balance throughout the shocked region, although CO is also a significant coolant.

VI. SUMMARY

We have discussed the physical and chemical processes operating in the cooling gas behind a dissociative molecular shock, and we have computed the structure of the shocked gas regions for shocks of velocity 60, 80, 90, and 100 km s^{-1} in gas of preshock density 10^4, 10^5, and 10^6 cm^{-3}. Our treatment has taken account of the conversion of Lyα photons into radiation of two-photon continuum and into H_2 Lyman band emission lines, and we have included the effects of photodissociation of CO by line absorption. We have presented the abundance profiles for the most abundant molecules composed of the elements hydrogen, helium, carbon, nitrogen, oxygen, silicon, and sulphur, and we have discussed the dependence of the molecular column densities on the shock velocity and preshock gas density. We have also investigated the sensitivity of our results to such parameters as the magnetic field strength, the assumed efficiency of molecular hydrogen formation on grain surfaces, and the elemental abundances.

Reformation of molecular hydrogen takes place before the gas temperature falls below a few hundred degrees, provided that H_2 formation on grains is at least as efficient as has been assumed by Hollenbach and McKee (1979). We find, however, that the precise shock structure is sensitive to uncertainties in the efficiency of the grain formation process.

Chemical processes in the warm shocked gas are effective in converting a substantial fraction of the metal atoms into the neutral molecules OH, H_2O, O_2, CO, CN, HCN, N_2, NO, SO, and SiO; the OH molecule plays a central role in the network of chemical reactions. With the exception of N_2, however, none of the enhanced abundances of these species persists after the gas has cooled below 200 K, because the endothermic production route to the crucial OH intermediate ceases to be effective at low temperature while the destructive effects of the shock-generated UV radiation field are still felt.

Because the 35 μm [Si II] line has been proposed as a diagnostic of the ionization produced in a dissociative shock, the silicon chemistry assumes a particular significance. For shocks of preshock density 10^5 cm^{-3}, Si^+ is efficiently converted to SiO unless the shock velocity is as large as 90 km s^{-1}. Our result is sensitive to the proportion of $SiOH^+$ dissociative recombinations that lead to SiO, a fraction which can only be estimated.

Photoionization prevents the hydrocarbon species from reaching substantial abundances in the shocked gas region unless the elemental abundance of carbon exceeds that of oxygen.

The molecular ions H_2^+, H_3^+, OH^+, SO^+, and CH^+ all become abundant in a region where the shocked gas has a temperature of several thousand degrees and is still partially ionized. When the shock velocity is as large as 100 km s^{-1}, HeH^+ is also produced. The effectiveness of electron impact excitation of molecular ions suggests that the environment in which they are produced may be favorable to the production of vibrational emission of detectable strength.

We are greatly indebted to John Raymond for making his atomic shock code available to us. Without such assistance we would have been unable to compute the radiation field incident upon the molecular portion of the cooling, postshock gas. We are also very grateful to Ewine van Dishoeck, who has provided us with valuable assistance in determining what the likely photodestructive effects of that radiation field must be, most particularly by communicating to us unpublished results relating to CO and CN photodissociation. It is also a pleasure to acknowledge helpful discussions with V. Buch, B. T. Draine, G. B. Field, D. J. Hollenbach, and C. F. McKee. This work was supported by NSF grant AST-86-17675. This project was brought to completion while D. A. N. was supported by a special NASA astrophysics theory program which funds the Center for Star Formation Studies.

REFERENCES

Adams, F. 1975, *Ap. J.*, **201**, 350.
Anicich, V. G., and Huntress, W. T. 1986, *Ap. J. Suppl.*, **62**, 553.
Bally, J., and Lane, A. P. 1982, *Ap. J.*, **257**, 612.
Beckwith, W., Persson, S. E., Neugebauer, G., and Becklin, E. E. 1978, *Ap. J.*, **223**, 464.
Binette, L., Dopita, M. A., and Touhy, I. R. 1985, *Ap. J.*, **297**, 476.
Black, J. 1978, *Ap. J.*, **222**, 125.
Buch, V. 1987, private communication.
Buch, V., and Dalgarno, A. 1989, in preparation.
Burke, J. R., and Hollenbach, D. J. 1983, *Ap. J.*, **265**, 223.
Chernoff, D. F., Hollenbach, D. J., and McKee, C. F. 1982, *Ap. J. (Letters)*, **259**, L97.
Dalgarno, A., and McCray, R. 1972, *Ann. Rev. Astr. Ap.*, **10**, 375.
Draine, B. T. 1980, *Ap. J.*, **241**, 1021.
———. 1986, *Ap. J.*, **310**, 408.
Draine, B. T., and Katz, N. 1986, *Ap. J.*, **306**, 655.
Draine, B. T., and Roberge, W. G. 1982, *Ap. J. (Letters)*, **259**, L91.
Draine, B. T., Roberge, W. G., and Dalgarno, A. 1983, *Ap. J.*, **264**, 485.
Drake, G. W. F., Victor, G. A., and Dalgarno, A. 1969, *Phys. Rev.*, **180**, 25.
Duley, W. W., and Williams, D. A. 1986, *M.N.R.A.S.*, **223**, 177.
Field, G. B., Rather, J. D. G., Aannestad, P. A., and Orszag, S. A. 1968, *Ap. J.*, **151**, 953.
Gautier, T. N., Fink, U., Treffers, R. R., and Larson, H. P. 1976, *Ap. J. (Letters)*, **207**, L129.
Gear, C. W. 1971, *Numerical Initial Value Problems in Ordinary Differential Equations* (Englewood Cliffs: Prentice-Hall).
Graff, M. M., and Dalgarno, A. 1987, *Ap. J.*, **317**, 432.
Green, S., Montgomery, J. A., and Thaddeus, P. 1974, *Ap. J. (Letters)*, **193**, L89.
Haas, M., Hollenbach, D. J., and Erickson, E. F. 1986, *Ap. J. (Letters)*, **301**, L57.
Hasegawa, T., and Akabane, K. 1984, *Ap. J. (Letters)*, **287**, L91.
Herbst, E. 1983, *Ap. J. Suppl.*, **53**, 41.
Hollenbach, D. J., and McKee, C. F. 1979, *Ap. J. Suppl.*, **41**, 555.
———. 1980, *Ap. J. (Letters)*, **241**, L47.
Hummer, D. G., and Kunasz, P. B. 1980, *Ap. J.*, **236**, 609.
Iglesias, E. R., and Silk, J. 1978, *Ap. J.*, **226**, 851.
Jones, M. E., Barton, S. E., Ellison, G. B., and Ferguson, E. E. 1986, *Chem. Phys. Letters*, **130**, 218.
Jura, M. 1974, *Ap. J.*, **191**, 375.
Leen, T. M., and Graff, M. M. 1988, *Ap. J.*, **325**, 411.
Letzelter, C., Eldelsberg, M., Rostas, F., Breton, J., and Thieblemont, B. 1987, *Chem. Phys.*, **114**, 273.
Kley, D. 1984, *J. Atmos. Chem.*, **2**, 203.
Mathis, J. S., Rumpl, W., and Nordsieck, K. H. 1977, *Ap. J.*, **217**, 425.
McKee, C. F., Chernoff, D., and Hollenbach, D. 1984, in *Proc. 16th ESLAB Symposium, Galactic and Extragalactic Infrared Spectroscopy*, ed. M. Kessler and J. Phillips (Dordrecht: Reidel), p. 103.
McKee, C. F., and Hollenbach, D. 1987, *Ap. J.*, **322**, 275.
McKee, C. F., Storey, J. W. V., Watson, D. M., and Green, S. 1982, *Ap. J.*, **259**, 647.
Melnick, G. J., Genzel, R., and Lugten, J. B. 1987, *Ap. J.*, **321**, 530.
Mendoza, C. 1983, in *IAU Symposium 103, Planetary Nebulae*, ed. D. R. Flower (Dordrecht: Reidel), p. 143.
Millar, T. J., Adams, N. G., Smith, D., Lindinger, W., and Villinger, H. 1986, *M.N.R.A.S.*, **221**, 673.
Mitchell, G. F. 1984, *Ap. J. Suppl.*, **54**, 81.
Mul, P. M., Mitchell, J. B. A., D'Angelo, V. S., Defrance, P., McGowan, J. W., and Froelich, H. R. 1981, *J. Phys. B*, **14**, 1353.
Neufeld, D. A. 1987, Ph.D. thesis, Harvard University.
Neufeld, D. A., and Dalgarno, A. 1989, *Phys. Rev. A.*, submitted.
Neufeld, D. A., and McKee, C. F. 1989, *Ap. J. (Letters)*, submitted.
Neufeld, D. A., and Melnick, G. 1987, *Ap. J.*, **322**, 266.
Osterbrock, D. E. 1974, *Astrophysics of Gaseous Nebulae* (San Francisco: Freeman).
Ostriker, J. P., and Cowie, L. L. 1981, *Ap. J. (Letters)*, **247**, L127.
Pineau des Forets, G., and Flower, D. R. 1987, *M.N.R.A.S.*, **228**, 1P.
Pineau des Forets, G., Flower, D., Hartquist, T. W., and Dalgarno, A. 1986, *M.N.R.A.S.*, **223**, 743.
Pineau des Forets, G., Flower, D. R., Hartquist, T. W., and Millar, T. J. 1987, *M.N.R.A.S.*, **227**, 993.
Pineau des Forets, G., Roueff, E., and Flower, D. R. 1986, *M.N.R.A.S.*, **223**, 743.
Raymond, J. C. 1979, *Ap. J. Suppl.*, **39**, 1.
Roberge, W., and Dalgarno, A. 1982, *Ap. J.*, **255**, 489.
Shull, J. M., and McKee, C. F. 1979, *Ap. J.*, **227**, 131.
Smith, D., and Adams, N. G. 1984, *Ap. J. (Letters)*, **269**, 329.
van Dishoeck, E. F. 1987, in *IAU Symposium 120, Astrochemistry*, ed. M. S. Vardya and S. P. Tarafdar (Dordrecht: Reidel), p. 51.
van Dishoeck, E. F., and Dalgarno, A. 1984, *Icarus*, **59**, 305.
Viala, Y. P., Letzelter, C., Eidelsberg, M., and Rostas, F. 1988, *Astr. Ap.*, **193**, 265.
Wagner, A. F., and Graff, M. M. 1987, *Ap. J.*, **317**, 423.
Watson, D. M., Genzel, R., Townes, C. H., and Storey, J. W. V. 1985, *Ap. J.*, **298**, 316.
Wilson, S. 1978, *Ap. J.*, **220**, 737.
Yoshino, K., Stark, G., Smith, P. L., Parkinson, W. H., and Ito, K. 1988, *J. Phys. (Paris)*, **49**, C1-37.

A. DALGARNO: Harvard-Smithsonian Center for Astrophysics, 60 Garden Street, Cambridge, MA 02138

D. A. NEUFELD: Department of Astronomy, University of California, Berkeley, CA 94720